UNDERWATER PROPAGATION OF SOUND WAVES EXCITED BY A POINT SOURCE ABOVE THE SURFACE

Wasyl Wasylkiewskyj

Institute for Defense Analyses

Prepared for:

Department of the Army

May 1974

The work reported in this document was conducted under contract DAHC15 73 C 0200 for the Department of Defense. The publication of this IDA Paper does not indicate endorsement by the Department of Defense, nor should the contents be construed as reflecting the official position of that agency.

UNCLASSIFIED

SECURITY CLASSIFICATION OF THIS PAGE (When Data Entered)

AD 783 009

REPORT DOCUMENTATION PAGE

READ INSTRUCTIONS BEFORE COMPLETING FORM

1. REPORT NUMBER: Paper P-999	2. GOVT ACCESSION NO. / 3. RECIPIENT'S CATALOG NUMBER
4. TITLE (and Subtitle): Underwater Propagation of Sound Waves Excited by a Point Source Above the Surface	5. TYPE OF REPORT & PERIOD COVERED: FINAL
	6. PERFORMING ORG. REPORT NUMBER: P-999
7. AUTHOR(s): Wasyl Wasylkiwskyj	8. CONTRACT OR GRANT NUMBER(s): DAHC15 73 C 0200
9. PERFORMING ORGANIZATION NAME AND ADDRESS: INSTITUTE FOR DEFENSE ANALYSES, 400 Army-Navy Drive, Arlington, Virginia 22202	10. PROGRAM ELEMENT, PROJECT, TASK AREA & WORK UNIT NUMBERS: Warning System Concepts
11. CONTROLLING OFFICE NAME AND ADDRESS: Director for Indications & Warning, ASD(I), The Pentagon, Washington, D.C. 20301	12. REPORT DATE: May 1974
	13. NUMBER OF PAGES: ~~66~~ 71
14. MONITORING AGENCY NAME & ADDRESS (if different from Controlling Office)	15. SECURITY CLASS (of this report): UNCLASSIFIED
	15a. DECLASSIFICATION/DOWNGRADING SCHEDULE: NONE

16. DISTRIBUTION STATEMENT (of this Report)

Distribution of this document is unlimited.

17. DISTRIBUTION STATEMENT (of the abstract entered in Block 20, if different from Report)

None

18. SUPPLEMENTARY NOTES

N/A

19. KEY WORDS (Continue on reverse side if necessary and identify by block number)

Propagation
Underwater Acoustics

20. ABSTRACT (Continue on reverse side if necessary and identify by block number)

This paper constitutes a technical support document to the IDA Paper P-1013 "Warning Systems Concepts" by R. Turner, and deals with the problem of obtaining first-order quantitative estimates of acoustic power coupling from sources above the ocean surface into regions deep within isothermal ocean layers. The systems implications of the analytical and numerical results

DD FORM 1 JAN 73 1473 EDITION OF 1 NOV 65 IS OBSOLETE

UNCLASSIFIED

SECURITY CLASSIFICATION OF THIS PAGE (When Data Entered)

20.

obtained herein are not discussed, but are treated in the main document; briefly, however, this analysis was motivated by the possibility of detecting acoustic radiation from aircraft with underwater sensors.

Of particular interest are ocean depths on the order of several kilometers, source-to-observation-point separations on the order of hundreds of kilometers, and source frequencies below 100 Hz. The analysis deals only with the classical planar layer model for the ocean. The ocean floor is assumed either perfectly reflecting or perfectly absorbing. Consequently, the results should prove of value in establishing lower and upper bounds on attainable acoustic signal strengths in an isothermal ocean at large ranges from above-surface sources. Particular emphasis is given to effecting quantitative comparisons of acoustic pressure in the ocean due to sources above and below the surface. Several "source equivalence" principles are discussed to facilitate such comparisons.

PAPER P-999

UNDERWATER PROPAGATION OF SOUND WAVES EXCITED BY A POINT SOURCE ABOVE THE SURFACE

Wasyl Wasylkiwskyj

May 1974

IDA
INSTITUTE FOR DEFENSE ANALYSES
SCIENCE AND TECHNOLOGY DIVISION
400 Army-Navy Drive, Arlington, Virginia 22202

Contract DAHC15 73 C 0200
Warning System Concepts

CONTENTS

I.	Introduction and Summary	1
II.	Analysis of Acoustic Wave Propagation in a Planar Layer	5
	A. General Integral Representations of the Acoustic Potential Due to a Point Source Near a Planar Layer	5
	B. Asymptotic Evaluation of the Integral for the Acoustic Potential for a Layer with a Constant Refractive Index	9
	C. Asymptotic Evaluation of Acoustic Potential for a Layer with a Linearly Varying Refractive Index Profile	32
	D. Acoustic Potential in a Layer with a Highly Absorbent Lower Boundary	39
III.	Propagation of Acoustic Signals Over Long Paths Below the Ocean Surface	54
	References	65

I. INTRODUCTION AND SUMMARY

The analytic investigation reported here deals primarily with the problem of obtaining first-order quantitative estimates of acoustic power coupled into regions near the ocean floor from sources located above the air-water interface. Of particular interest are ocean depths on the order of several kilometers, source-to-observation-point separations on the order of hundreds of kilometers, and acoustic source frequencies below 100 Hz. Even though a wealth of experimental and analytic data are available in the technical literature pertaining to acoustic wave propagation below the sea surface, they appear to be either not directly applicable to the parameter range of interest herein, or are not in a suitable form for extracting numerical information. In particular, a preponderant number of analyses deals with wave propagation excited by submerged sources.

The problem of acoustic energy coupling from sources above the ocean surface to a distant receiver located near the ocean bottom is, admittedly, too complex to be amenable to a reasonably bounded mathematical treatment. Usual analytical approaches in theoretical underwater acoustics focus on analyses of grossly simplified models which, hopefully, include the dominant features affecting one or more parameters of interest. Classically, to the first order of approximation, the ocean has been modeled as an infinite, perfectly smooth planar layer with an appropriate acoustic velocity profile. In addition, the ocean bottom is usually assumed perfectly smooth and characterized by a constant surface impedance, thus neglecting the boundary irregularities at the ocean bottom contours. The latter approximation has proven quite acceptable for certain shallow water channels and short propagation paths. For long propagation paths the assumption of a perfectly flat ocean floor appears much less realistic, since rather wide variations

in the ocean bottom contours may be encountered. Past analytical studies of long-range acoustic propagation phenomena in deep oceans have tended to neglect the effects of the sea bottom. This is permissible in a sufficiently deep ocean if the receiver and transmitter are located well above the ocean floor and the dominant propagation mechanism is either that of "ducting" of acoustic energy by virtue of the velocity profile associated with thermoclines near the ocean surface, or of multiple reflections of rays from the equivalent ocean surface and main thermocline discontinuity. The latter propagation mechanism is that traditionally associated with SOFAR (Ref. 1, p. 132). In the problem of interest here, the receiver is located in the deep isothermal layer close to the ocean floor while the transmitter is above the ocean surface. Consequently, the effects of sea bottom may play a significant role in determining the acoustic pressure at the receiver. A sufficiently realistic model, taking account of the irregularities of the ocean bottom would be analytically intractable. On the other hand, a combination of analytical and numerical techniques would make the results too dependent on the choice of specific ocean contours. In light of these difficulties, the approach adopted here is to consider propagation in the isothermal ocean layer with the lower boundary conforming to one of the two limiting conditions: a perfectly smooth, acoustically hard boundary, or a perfect absorber. The former model can be considered to correspond to an optimum set of propagation conditions for enhancing acoustic signals by systematic reflections from the ocean floor. The second model yields acoustic signals arriving at the distant receiver site only by virtue of ray caustics and multiple reflections at the ocean surface, since the rays impinging on the perfect absorber are not reflected. The perfect absorber model, then, yields a lower bound on the attainable signal strengths at the receiver site. The results derived on the basis of these two models can provide quantitative estimates of bounds on attainable signal strengths over long propagation paths as well as some estimates of the role played by systematic reflections from the ocean floor in signal enhancement. Also, the results should prove of value in effecting comparisons between acoustic signal strengths in the ocean

arising from submerged sources and those attributable to sources above the air-water interface. While data dealing with the former case are abundant, the latter does not appear to have received a comparable amount of attention. Consequently, quantitative comparisons of propagation characteristics of acoustic wave types in the ocean launched by a source above the ocean surface with those due to an "equivalent" submerged source merit attention even for rather idealized propagation conditions.

A portion of this paper (Sections A through C of Chapter II) is devoted to a detailed and somewhat tutorial exposition of acoustic wave propagation in a planar layer which, as mentioned in the preceding, constitutes the model adopted for the ocean. While much of this material could have been extracted from several well-known texts on wave propagation (notably Refs. 2 and 3), the treatments there are rather general, with the final results frequently not in the form most suitable for the parameter range of present interest. It was, therefore, felt desirable to develop various alternative representations for the acoustic wave function, with the immediate application firmly in mind. Such a self-contained treatment also provides for a degree of uniformity in notation and nomenclature.

Sections A through C of Chapter II contain a discussion of asymptotic representations of the acoustic potential deriving from a point source above a planar layer. Relative merits of the ray and leaky-wave (mode) series are discussed from a numerical computational standpoint. Of the two, the leaky-wave series has been found more suitable for application to long propagation paths. The final forms of these series, including the simplifications applicable to the specific parameter range of interest, are given in Eq. 65 for the constant refractive index profile and in Eq. 78 for the linearly varying profile. In both cases, the ocean bottom is modeled as an acoustically hard, flat surface. The layer with a perfectly absorbent lower boundary is discussed in Section D of Chapter II, where the leaky wave series, Eq. 96, is found to converge very rapidly for observation points near the lower layer boundary. Since one of the objects of this study is to

make quantitative comparisons of acoustic pressure produced by sources above the ocean surface with those located in the water, Section E of Chapter II is devoted to a parallel development of residue series representations for the potential due to a submerged point source.

Chapter III contains the application of the preceding results to underwater acoustic propagation. With regard to the relative acoustic pressure produced by submerged and above-surface sources, it was found that a point source above the ocean surface will give rise to a pressure about 800 times as large as that due to a submerged point source of equal strength close to the air-water interface. This result holds only for observation points sufficiently far removed from the source, but is only very weakly dependent on the height of the source above the ocean. As the submerged source is moved further below the air-water interface, this "equivalent" source principle no longer applies. Instead, direct calculations reveal that the pressures produced by a submerged and above-surface source are of the same order of magnitude, provided the two sources are of equal strength and the ocean bottom is assumed perfectly reflecting. This result is also practically independent of the height of the source above the water surface. For the case of an acoustically hard bottom, numerical results are presented for the acoustic pressure at various propagation ranges for sources above and below the surface (Figs. 2 through 6). When the ocean bottom is assumed perfectly absorbing, the pressure produced by a submerged source is considerably higher (by 24 db) than that produced by a source above the water, showing, by comparison with the results for a perfectly reflecting bottom, that systematic reflections at the ocean floor can result in a substantial enhancement of acoustic signals generated by above-surface sources for the propagation paths in question. The relationship between average acoustic pressures for submerged and above-surface sources is particularly simple if the ocean bottom is assumed perfectly absorbing. This relationship is given by Eq. 123. Also, for a perfectly absorbent bottom, the average pressure is shown to obey the cylindrical spreading law with range ($1/\sqrt{\rho}$) and the expressions for the average pressure at great distances from the source reduce to the rather simple algebraic forms given in Eqs. 120 and 121.

II. ANALYSIS OF ACOUSTIC WAVE PROPAGATION IN A PLANAR LAYER

A. GENERAL INTEGRAL REPRESENTATIONS OF THE ACOUSTIC POTENTIAL DUE TO A POINT SOURCE NEAR A PLANAR LAYER

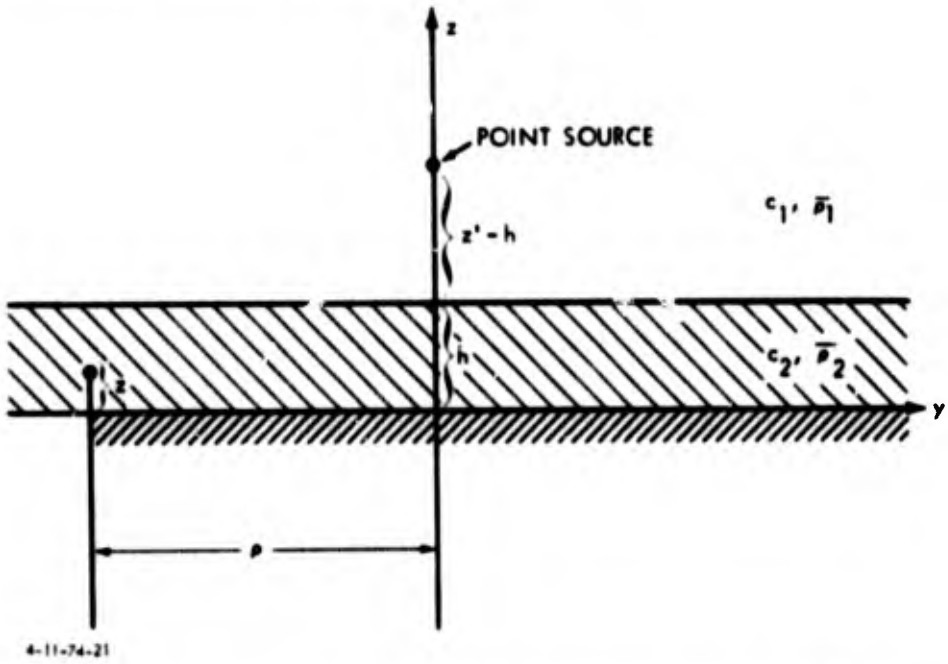

Consider an acoustic point source above a planar layer of height h bounded at z = 0 by a perfectly rigid infinite plane, as shown in the sketch above. The speed of sound c_1 and density $\bar{\rho}_1$ pertaining to the upper medium are assumed constant. In the lower medium, the density $\bar{\rho}_2$ is also constant, but the speed of sound c_2 may vary with z. Denoting the acoustic potential by Ψ, and assuming a time harmonic source $e^{-i\omega t}$ of unit strength, the wave equation satisfied by Ψ is

$$\left(\nabla^2 + \frac{\omega^2}{c_1^2}\right) \Psi_1 = -\delta(x)\,\delta(y)\,\delta(z-z') \; ; \; h \le z < \infty \; , \qquad (1a)$$

and

$$\left(\nabla^2 + \frac{\omega^2}{c_2^2}\right) \Psi_2 = 0 \; ; \; 0 \le z \le h \; . \tag{1b}$$

The potential function Ψ is related to the acoustic pressure p by

$$p_{1,2} = -i\omega \, \bar{\rho}_{1,2} \, \Psi_{1,2} \; , \tag{2}$$

and satisfies the following boundary conditions

$$\bar{\rho}_1 \Psi_1 = \bar{\rho}_2 \Psi_2 \; , \quad \frac{\partial \Psi_1}{\partial z} = \frac{\partial \Psi_2}{\partial z} \quad \text{at } z = h \; , \tag{3a}$$

$$\frac{\partial \Psi_2}{\partial z} = 0 \quad \text{at } z = 0 \; . \tag{3b}$$

In addition, Ψ must satisfy the outgoing wave (radiation) condition for $z \to \infty$.

The solution of Eq. 1 can be represented in a variety of forms. For computing Ψ in the lower medium at large radial distances ρ from the source point (Fig. 1), a suitable representation involves the Hankel transform in the ρ coordinate. Thus, one can write

$$\Psi(\rho, z, z') = \frac{1}{2\pi} \int_0^\infty dK \, K J_0(K\rho) \, g(z, z'; \kappa_1) \; , \tag{4}$$

where g is an appropriate one-dimensional Green's function in the z domain. The variable of integration K is the transverse wave number corresponding to the angle of incidence w in medium 1 for a typical plane wave entering into the superposition integral (Eq. 4). When w is defined with respect to the normal of the planar interface, one has

$$K = k_1 \sin w \; , \; k_1 = \frac{\omega}{c_1} \; . \tag{5}$$

The quantity $\varkappa_1$ in Eq. 4 is the plane wave propagation constant relative to the z direction in medium 1, and is related to K by

$$\varkappa_1 = \sqrt{k_1^2 - K^2} \quad , \; k_1 = \frac{\omega}{c_1} \; . \tag{6}$$

For observation points in medium 2, the one-dimensional Green's function $g(z,z';\varkappa_1)$ is

$$g(z,z';\varkappa_1) \tag{7}$$

$$= \frac{\bar{\rho}_1 \, e^{i\varkappa_1(z'-h)} \left[\dot{f}_1(0)f_2(z) - \dot{f}_2(0)f_1(z)\right]}{i\,\bar{\rho}_2\,\varkappa_1\left[\dot{f}_2(0)f_1(h) - \dot{f}_1(0)f_2(h)\right] + \bar{\rho}_1\left[\dot{f}_1(0)\dot{f}_2(h) - \dot{f}_2(0)\dot{f}_1(h)\right]}$$

where $f_1(z)$, $f_2(z)$ are any two linearly independent solutions of

$$\left[\frac{d^2}{dz^2} + \varkappa_2^2(z)\right] \; f_{1,2}(z) = 0 \tag{8}$$

$$\varkappa_2(z) = \sqrt{k_2^2(z) - K^2} \; ; \; k_2(z) = \frac{\omega}{c_2(z)} \quad , \tag{9}$$

and

$$\dot{f}_{1,2}(z) \equiv \frac{d}{dz} f_{1,2}(z) \; .$$

Eq. 4, in conjunction with Eqs. 7 and 8, constitutes a complete formal solution for the acoustic potential in medium 2. However, numerical computation of Ψ for a given set of medium and geometrical parameters entails a number of difficulties. One of these is the solution of Eq. 8, the other is the evaluation of the integral in Eq. 4. The differential equation for $f_{1,2}(z)$ can be solved in terms of known functions in only a limited number of cases, viz., refractive

index profiles $n(z) = k_2(z)/k_1$ for which Eq. 8 reduces to a special form of the hypergeometric equation. Only when the refractive index varies slowly relative to the local wavenumber, that is, when $\dot{k}_2(z)/k_2(z) \ll k_1$, can Eq. 8 be solved for arbitrary functional forms of $k_2(z)$. This can be done by employing the WKB approximation, valid for z sufficiently far removed from the turning points of the differential equation, viz., the zeros of $\varkappa_2(z)$. With the aid of these approximate forms, the integral (Eq. 4) can be evaluated asymptotically for large k_1, yielding the geometrical acoustics ray solution as well as diffraction effects associated with caustics and focal points.

For present purposes, the refractive index profiles of interest are $k_2(z) = k_2 =$ constant and

$$k_2^2(z) = k_1^2 \left[N^2 - a(h - z)\right] , \tag{10}$$

that is, a linear function of z. In the first instance, the solutions of Eq. 8 are exponentials, while in the second instance they are Airy functions. Thus, for a constant refractive index

$$f_{1,2}(z) = e^{\pm i\varkappa_2(z-h)} , \tag{11}$$

which, substituted in Eq. 7, yields

$$g(z,z';\varkappa_1) = im\, e^{i\varkappa_1(z'-h)} \frac{e^{i\varkappa_2(h+z)} + e^{i\varkappa_2(h-z)}}{(\varkappa_1 - m\varkappa_2)\, e^{i2\varkappa_2 h} + (\varkappa_1 + m\varkappa_2)} , \tag{12}$$

where

$$m = \frac{\bar{\rho}_1}{\bar{\rho}_2} .$$

For the linearly varying refractive index profile, a set of linearly independent functions of Eq. 8 is

$$f_1(z) = \mathrm{Ai}\left[\left(k_1^2 a\right)^{1/3}(z_p - z)\right] \quad , \tag{13a}$$

$$f_2(z) = \mathrm{Bi}\left[\left(k_1^2 a\right)^{1/3}(z_p - z)\right] \quad , \tag{13b}$$

where Ai, Bi are Airy functions (Ref. 3), and

$$z_p = h - \left(\frac{k_1^2 N^2 - K^2}{k_1^2 a}\right) \quad . \tag{14}$$

Substitution of Eq. 13 into Eq. 7 yields, together with Eq. 4, an integral representation for the acoustic potential in a medium with a linearly varying refractive index profile.

Once the integrand in Eq. 4 has been expressed in closed form, there remains the problem of evaluating the integral, which evidently cannot be expressed in terms of tabulated functions. One can, of course, always resort to numerical integration. However, such a procedure is not always practical. For example, if, as in the present case, the potential is to be computed at large distances from the source point, the rapidly oscillating term $J_o(K\rho)$ in the integrand would require an extremely large number of grid points for even a modest accuracy. The problem is further complicated if the layer thickness h is large in terms of wavelengths, since the one-dimensional Green's function, Eq. 7, will, in this case, also involve rapidly oscillating functions. The usual approach in such cases is to effect an asymptotic evaluation of the integral for large ρ and (or) h. In the following discussion, the asymptotic evaluation is carried out in detail for the case of constant $k_2(z)$, and the results are subsequently extended to a linearly varying refractive index profile.

B. ASYMPTOTIC EVALUATION OF THE INTEGRAL FOR THE ACOUSTIC POTENTIAL FOR A LAYER WITH A CONSTANT REFRACTIVE INDEX

As the first step toward an asymptotic evaluation of the integral in Eq. 4, one must examine all singularities of the integrand in the

complex K plane. For this purpose, it is convenient to transform the Bessel function $J_o(K\rho)$ into Hankel functions $H_o^{(1)}(K\rho)$, $H_o^{(2)}(K\rho)$ with the aid of $2J_o(K\rho) = H_o^{(1)}(K\rho) + H_o^{(2)}(K\rho)$. Employing the "circuit" relation

$$H_o^{(2)}(K\rho) = -H_o^{(1)}(K\rho e^{i\pi}) ,$$

and Eq. 12, the integral, Eq. 4, can be written in terms of $H_o^{(1)}(K\rho)$ alone:

$$\Psi(\rho,z,z') = \frac{im}{4\pi}\int_{-\infty}^{\infty} dK\, \frac{K}{i\pi} H_o^{(1)}(K\rho)\, \frac{e^{i\varkappa_1(z'-h)}\left[e^{i\varkappa_2(h+z)} + e^{i\varkappa_2(h-z)}\right]}{(\varkappa_1 - m\varkappa_2)\, e^{i2\varkappa_2 h} + (\varkappa_1 + m\varkappa_2)} . \quad (15)$$

The integrand in Eq. 15 contains branch point singularities at $K = 0$, corresponding to $H_o^{(1)}(K\rho)$, as well as branch points of $\varkappa_1 = \sqrt{k_1^2 - K^2}$ at $K = \pm k_1$. The propagation constant $\varkappa_2 = \sqrt{k_2^2 - K^2}$ in the lower medium does not contribute any branch points, since the integrand is an even function of $\varkappa_2$. In addition, the integrand may contain pole singularities in the complex K plane corresponding to the zeros of

$$(\varkappa_1 - m\varkappa_2)\, e^{i2\varkappa_2 h} + (\varkappa_1 + m\varkappa_2) = 0 . \quad (16)$$

These zeros can be subsumed under two categories: those lying in the region Im $\varkappa_1 > 0$, corresponding to the region of exponential decay of the integrand for large $|K|$, and those for which Im $\varkappa_1 < 0$. The former are referred to as "proper," or surface wave poles, the latter "improper," or leaky wave poles of the integrand. Choosing the branch cuts of $\sqrt{k_1^2 - K^2}$ such that Im $\varkappa_1 > 0$ on the entire top Riemann sheet, the disposition of the path of integration in Eq. 15 relative to all of the above singularities is shown in Fig. 1.

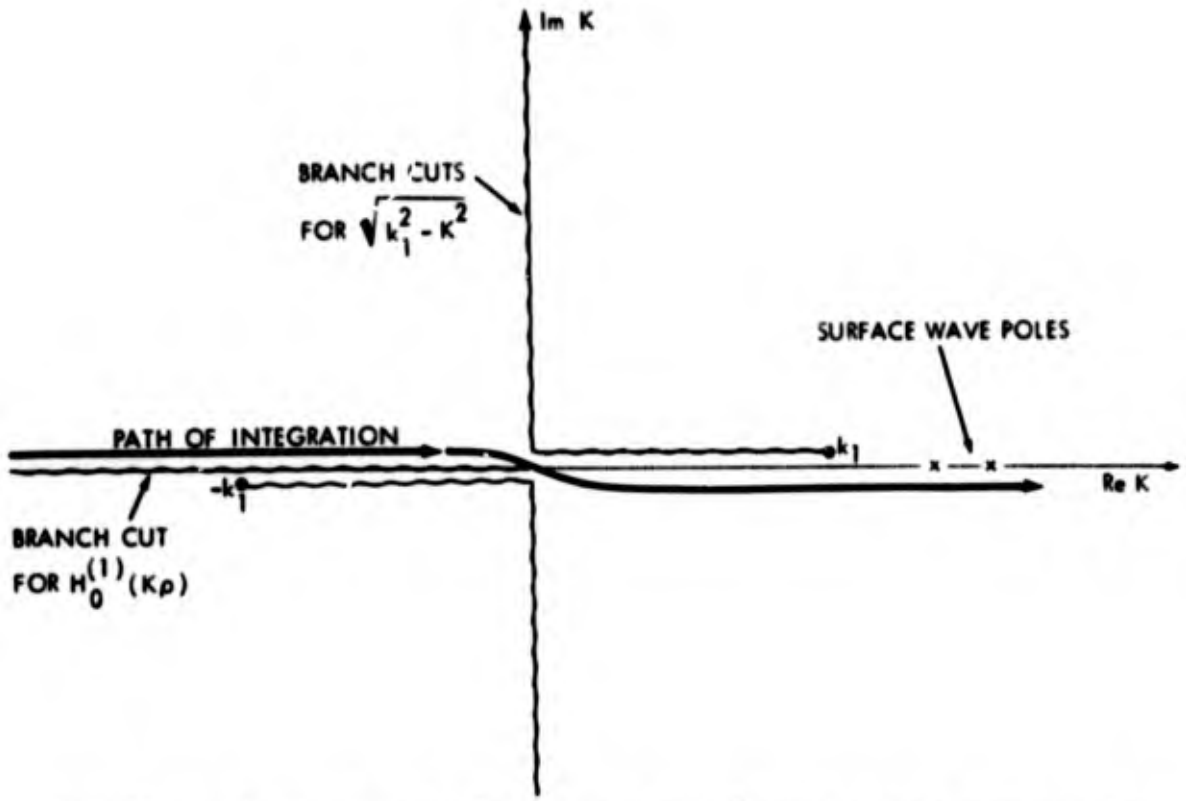

FIGURE 1. Disposition of the Path of Integration Relative to Singularities of the Integrand (Eq. 15)

$$\left(\text{Im}\sqrt{k_1^2 - K^2} \geq 0 \text{ on the entire top Riemann sheet}\right)$$

Due to the choice of branch cuts of $\sqrt{k_1^2 - K^2}$, only surface wave poles appear on the top Riemann sheet, the leaky wave poles being confined to the lower sheet. The surface wave poles correspond to characteristic modes guided by the discontinuity between the two media. For dissipationless media, such poles are confined to the real K axis ($|\text{Re } K| > k_1$), contributing to guided waves propagating without attenuation along the radial direction. The contribution of these surface waves to the total acoustic potential can be exhibited explicitly by recasting Eq. 15 into a representation involving characteristic modes propagating along the ρ direction. Such a representation can be obtained by deforming the path of integration in Fig. 1 around the branch and pole singularities in the upper half of the complex K plane. This path deformation is permissible, since the contribution to the integral from the infinite semicircle ($|K| \to \infty$) vanishes by virtue

of the condition Im $\varkappa_1 > 0$. The deformed path is shown in the illustration below.

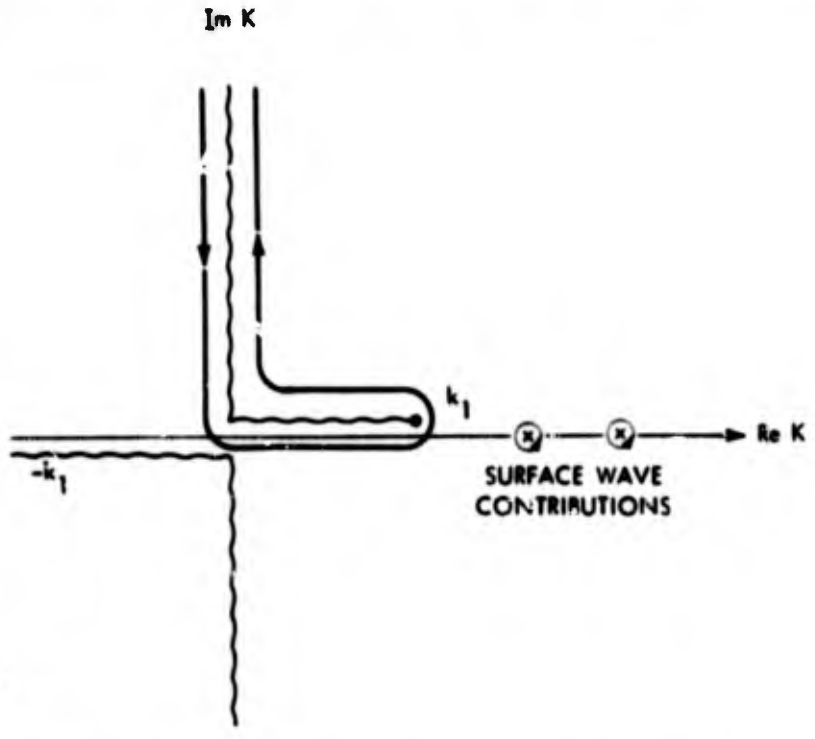

Integrating around the branch cut and the (simple) pole singularities, and noting that Re $\varkappa_1 \gtrless 0$ on the left and right of the cut, respectively, one obtains

$$\Psi = \frac{im}{4\pi}\int_{-\infty}^{\infty} d\xi\, e^{i\xi(z'-h)}\, \frac{\xi \cos(\varkappa_2 \xi)}{\xi \cos \varkappa_2 h - im\varkappa_2 \sin \varkappa_2 h}\, H_0^{(1)}\left(\sqrt{k_1^2 - \xi^2}\,\rho\right) \quad (17)$$

$$- \frac{m}{2}\sum_{\ell} K_\ell\, \frac{e^{i\varkappa_{1\ell}(z'-h)}\left[e^{i\varkappa_{2\ell}(h+z)} + e^{i\varkappa_{2\ell}(h-z)}\right]}{\frac{d}{dK}\left[(\varkappa_1 - m\varkappa_2)\, e^{i2\varkappa_2 h} + (\varkappa_1 + m\varkappa_2)\right]_{K=K_\ell}}\, H_0^{(1)}(K_\ell \rho)\,,$$

where the K_ℓ are roots of Eq. 16. The integral in Eq. 17 corresponds to modes of the continuous spectrum, while the series corresponds to modes of the discrete spectrum, i.e., surface waves. In the case of the continuous spectrum, the modes travel in the radial direction as cylindrical waves $H_0^{(1)}\left(\sqrt{k_1^2 - \xi^2}\,\rho\right)$, and for each ξ there corresponds a

mode. Modes with $\xi < k_1$ are propagating, while those with $\xi > k_1$ are evanescent, since in the latter case $\sqrt{k_1^2 - \xi^2} = +i\sqrt{\xi^2 - k_1^2}$, and the Hankel function decays exponentially. Thus, the dominant contribution to the integral will arise from modes having indices $|\xi| < k_1$. The series of surface waves will generally contain a finite number of terms. These waves also possess a cylindrical character in the radial direction, i.e., $H_0^{(1)}(K_\ell \rho)$, but due to real K_ℓ, propagate without attenuation.* The representation in Eq. 17 offers an advantage over Eq. 15 only if the surface wave contribution is dominant, since the direct numerical evaluation of the integrals in both cases is subject to the same difficulties.

To effect an asymptotic evaluation of Eq. 15 for large ρ, it is convenient to change the variable of integration in Eq. 15 from K to w with the aid of the transformation in Eq. (5), thus eliminating the branch point singularities at $K = k_1$. The integral can then be written as

$$V = \frac{imk_1^2}{4\pi} \int_P \sin w \cos w \, e^{ik_1(z'-h)\cos w} \, T(w) \, H_0^{(1)}(k_1 \rho \sin w) \, dw, \qquad (18)$$

where

$$T(w) = \frac{e^{i\varkappa_2(h+z)} + e^{i\varkappa_2(h-z)}}{(\varkappa_1 - m\varkappa_2)\, e^{2ih\varkappa_2} + (\varkappa_1 + m\varkappa_2)} \qquad (19)$$

$$\varkappa_1 = k_1 \cos w, \quad \varkappa_2 = k_1 \sqrt{n^2 - \sin^2 w}, \quad n = \frac{k_2}{k_1} .$$

The path of integration in the w plane is shown in the sketch on page 14, where in the shaded regions Im $k_1 \cos w > 0$.

*Excluding the "cylindrical spreading" of $H_0^{(1)}(K_\ell \rho)$ as $1/\sqrt{\rho}$ for large ρ.

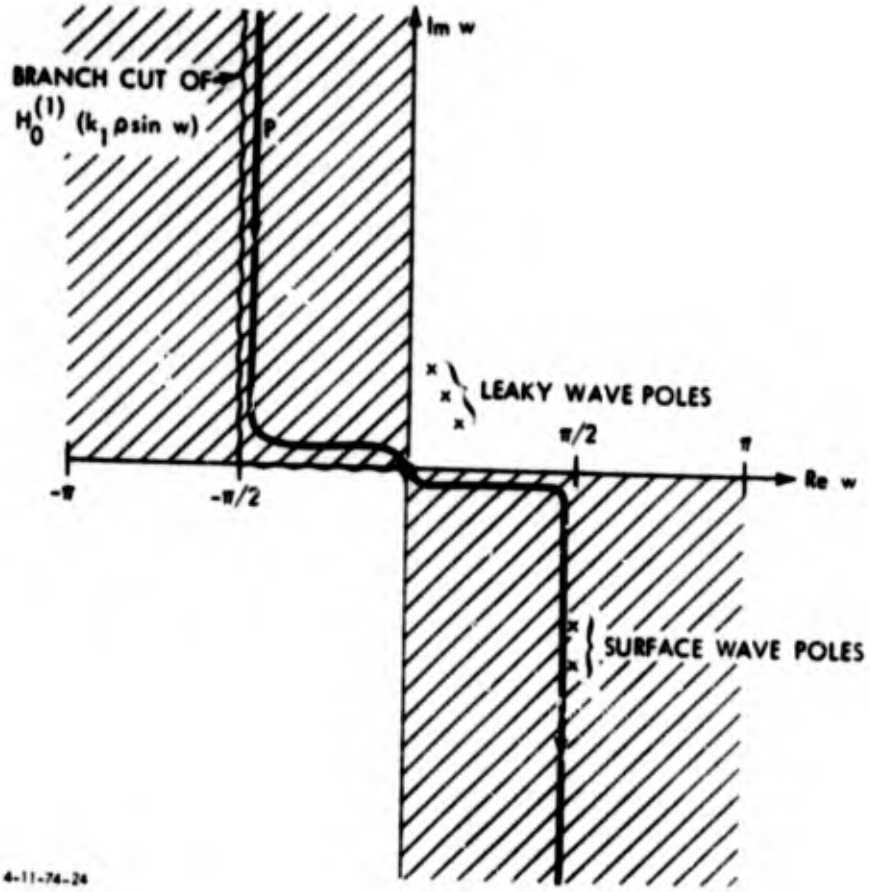

In the unshaded regions ($0 < \text{Re } w < \pi$, $\text{Im } w > 0$) and ($\pi < \text{Re } w < 0$, $\text{Im } w < 0$), one has $\text{Im } k_1 \cos w < 0$, which, evidently, corresponds to the bottom Riemann sheet in the complex K plane of Fig. 1. The path of integration can always be deformed away from $w = 0$, so that for large $k_1\rho$ the Hankel function in Eq. 18 may be written in terms of its asymptotic form:

$$H_0^{(1)}(k_1\rho\sin w) \sim \sqrt{\frac{2}{\pi k_1 \rho \sin w}}\, e^{-i\pi/4}\, e^{ik_1\rho\sin w}, \qquad (20)$$
$$k_1\rho\sin w \sim \infty$$

Thus, for large $k_1\rho$, one can write

$$\Psi = \frac{imk_1^2}{4\pi}\sqrt{\frac{2}{\pi k_1\rho}}\, e^{-i\pi/4} \qquad (21)$$
$$\int_P \sqrt{\sin w}\, \cos w\, T(w)\, e^{ik_1(z'-h)\cos w + ik_1\rho\sin w}\, dw .$$

Eq. 21 is the required form for asymptotic evaluation.

The first asymptotic result to be derived is the ray series of geometrical acoustics. To this end one expands T(w) in Eq. 19 in a geometric series

$$T(w,z) = \frac{1}{\varkappa_1 + m\varkappa_2} \left[e^{i\varkappa_2(h+z)} + e^{i\varkappa_2(h-z)} \right] \sum_{\ell=0}^{\infty} (-1)^{\ell} \left(\frac{\varkappa_1 - m\varkappa_2}{\varkappa_1 + m\varkappa_2} \right)^{\ell} e^{i2\ell h\varkappa_2} , \tag{22}$$

which converges, provided Im $\varkappa_2 > 0$. Substituting this in Eq. 21, one can write the result in the following form:

$$\Psi = \frac{imk^2}{4\pi} \sqrt{\frac{2}{\pi k_1 \rho}}\, e^{-i\pi/4} \int_P \frac{\sqrt{\sin w}\, \cos w}{\varkappa_1 + m\varkappa_2} \sum_{\ell=0}^{\infty} (-1)^{\ell} \left(\frac{\varkappa_1 - m\varkappa_2}{\varkappa_1 + m\varkappa_2} \right)^{\ell} \left[e^{ik_1\rho q_{\ell}^{+}(w)} + e^{ik_1\rho q_{\ell}^{-}(w)} \right] dw , \tag{23}$$

where

$$q_{\ell}^{\pm}(w) = \sin w + \frac{z'-h}{\rho} \cos w + \sqrt{n^2 - \sin^2 w} \left[\frac{(2\ell+1)h \pm z}{\rho} \right] \tag{24}$$

$$\ell = 0, 1, 2, \ldots .$$

The preceding can be expressed in a more compact form:

$$\Psi = e^{-i\pi/4} \frac{imk_1^2}{4\pi} \sum_{\ell=0}^{\infty} \left(I_{\ell}^{+} + I_{\ell}^{-} \right) , \tag{25}$$

$$I_{\ell}^{\pm} = \sqrt{\frac{2}{\pi k_1 \rho}} \int_P F_{\ell}(w)\, e^{ik_1\rho q_{\ell}^{\pm}(w)}\, dw , \tag{26}$$

$$F_{\ell}(w) = \frac{\sqrt{\sin w}\, \cos w}{\varkappa_1 + m\varkappa_2} (-1)^{\ell} \left(\frac{\varkappa_1 - m\varkappa_2}{\varkappa_1 + m\varkappa_2} \right)^{\ell} . \tag{27}$$

Eq. 25 gives Ψ as an infinite series of integrals, each containing the large parameter $k_1\rho$ in the exponent. Before evaluating these integrals by the method of steepest descents, one must examine the

singularities of $F_\ell(w)$ in the complex w plane. First, unlike the original integrand, Eq. 18, $F_\ell(w)$ possesses branch points at $\varkappa_2 = k_1\sqrt{n^2 - \sin^2 w} = 0$, or,

$$\sin w_p = \pm n \ . \tag{28}$$

It will be assumed that the speed of sound in the lower medium is greater than in the upper medium. Hence, $n < 1$ and the branch points are situated on the real w axis in the interval $0<|w_p|< \pi/2$. The positive w_p is identical with the angle of total reflection for a plane wave incident from medium 1 (compare Eq. 5). The only possible pole singularities are solutions of $\varkappa_1 + m\varkappa_2 = 0$. Denoting the zeros by w_p, one has

$$\sin w_p = \left[\frac{1 - m^2n^2}{1 - m^2}\right]^{\frac{1}{2}} \ . \tag{29}$$

With medium 2 denser than medium 1, $m < 1$. The case of special interest is $m << 1$, which yields $w_p \approx \pm \pi/2$.

When the path of integration P in Eq. 26 is deformed into the path of steepest descents $P_\ell^{\pm}$ (for each ℓ), its disposition relative to the singularities is as shown in the illustration on page 17. The deformation of P into $P_\ell^{\pm}$ is permissible, as long as no singularities are intercepted in the process.

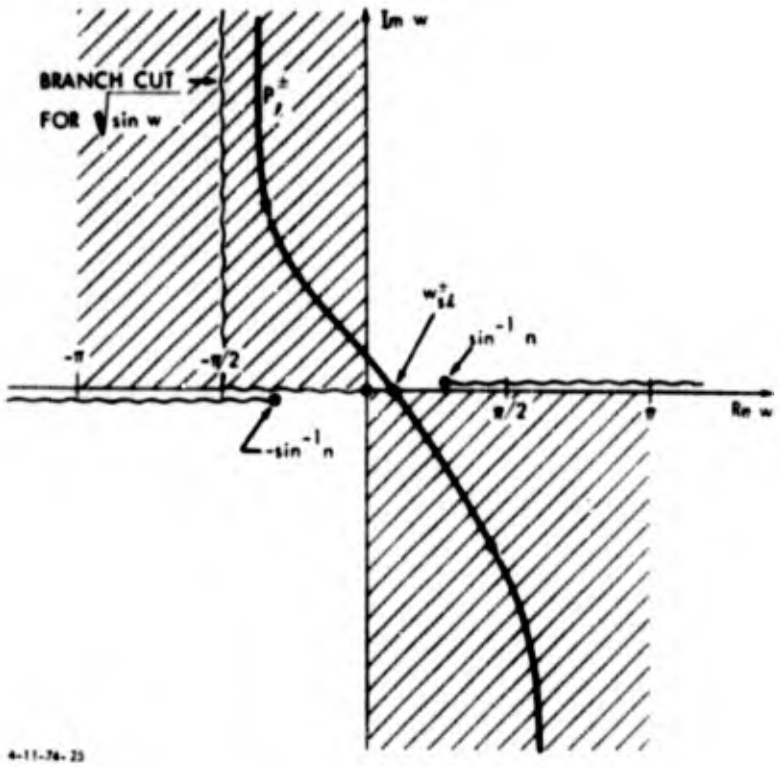

The branch cuts of $\sqrt{n^2 - \sin^2 w}$ have been chosen such that $\mathrm{Im}\sqrt{n^2 - \sin^2 w} > 0$ in the second and fourth quadrants, ensuring the convergence of the geometric series (Eq. 22) on the entire integration path. Moreover, the paths $P_\ell^\pm$ terminate in the shaded quadrants in the w plane, where Im cosw > 0, as required for convergence of the original integral, Eq. 21. The saddle points $w_{s\ell}^\pm$ are solutions of $\frac{d}{dw} q_\ell^\pm(w) = 0$. Employing Eq. 24, this is equivalent to

$$\frac{dq_\ell^\pm(w)}{dw} \equiv \dot{q}_\ell^\pm(w) = \cos w - \frac{z'-h}{\rho} \sin w \qquad (30)$$

$$-\left[\frac{(2\ell+1)h \pm z}{\rho}\right] \frac{\cos w \sin w}{[n^2 - \sin^2 w]^{\frac{1}{2}}} = 0 \ .$$

Thus $w_{s\ell}^\pm$ are determined from

$$\rho\sqrt{n^2 - \sin^2 w_{s\ell}^\pm} \cos w_{s\ell}^\pm = \sqrt{n^2 - \sin^2 w_{s\ell}^\pm}\,(z'-h) \sin w_{s\ell}^\pm \qquad (31)$$

$$+ [(2\ell+1)h \pm z] \cos w_{s\ell}^\pm \sin w_{s\ell}^\pm \ .$$

The preceding can be given a simple geometrical interpretation. Referring to the following sketch,

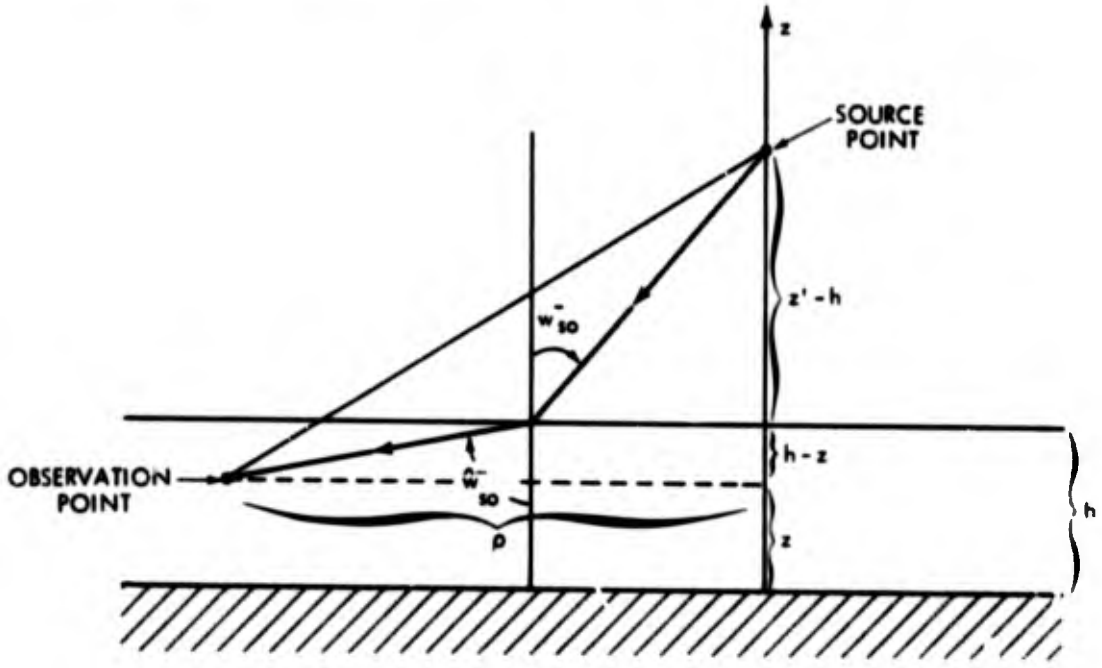

4-11-74-26

one notes from the geometry that

$$(z'-h) \tan w_{so}^- + (h-z) \tan \hat{w}_{so}^- = \rho \ ,$$

which may also be written in the following form:

$$(z'-h) \sin w_{so}^- \cos \hat{w}_{so} + (h-z) \cos w_{so}^- \sin \hat{w}_{so} = \rho \cos w_{so}^- \cos \hat{w}_{so}^- \ . \qquad (32)$$

Eq. 32 is equivalent to Eq. 31 for w_{so}^-, provided $\hat{w}_{so}^-$ is chosen in accordance with $\sin w_{so}^- = n \sin \hat{w}_{so}$, i.e., Snell's law of refraction. This leads to

$$n \cos \hat{w}_{so}^- = \sqrt{n^2 - \sin^2 w_{so}^-} \ ,$$

showing that for w_{so}^{-} Eq. 31 yields the equation of the direct refracted ray path between the source and observation points, depicted in the sketch on page 18. Similarly, one can show that for w_{so}^{+}, Eq. 31 represents the path of a ray reaching the observation point after a single reflection at the ground plane z = 0. The saddle points $w_{s\ell}^{+}$ for $\ell > 0$ correspond to rays which undergo multiple reflections at the ground plane and medium interface z = h. Ray paths for w_{so}^{-}, w_{so}^{+}, w_{s1}^{-}, and w_{s1}^{+} are shown in the illustration below.

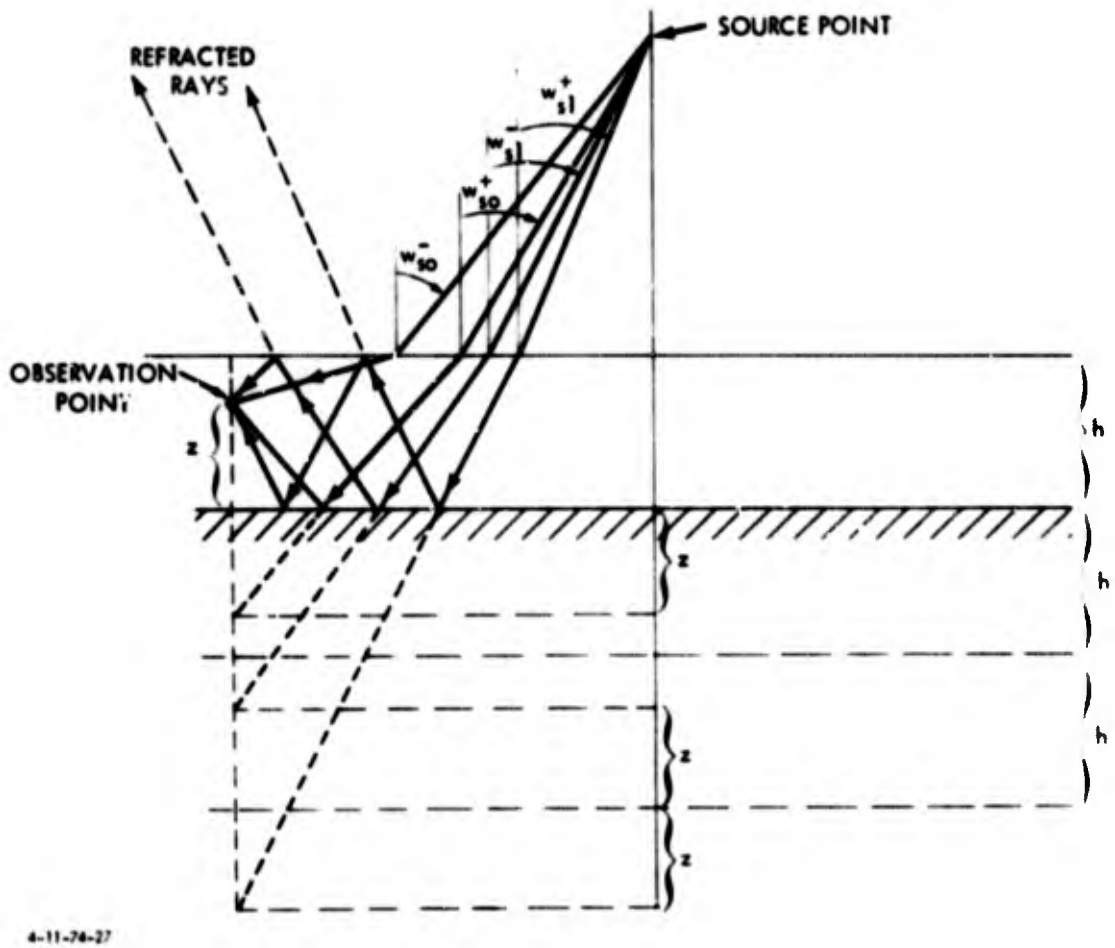

From the geometry one readily deduces the equivalence of Eq. 31 with the appropriate ray path. Note that for $\ell \neq 0$ the saddle points $w_{s\ell}^{-}$ and $w_{s\ell}^{+}$ pertain to rays which undergo their last reflection at the upper or lower boundary of medium 2, respectively. In view of

the geometrical interpretation of Eq. 31, it is evident that for a given ρ, z, there exists an infinite set of real solution $w_{s\ell}^{\pm}$, or, equivalently, that any fixed observation point in medium 2 is accessible by means of an infinite number of ray paths. The saddle points $w_{s\ell}^{\pm}$ are identical with the angles of incidence of rays in medium 1, and can be ordered in the decreasing sequence

$$w_{so}^{-} > w_{so}^{+} > w_{s1}^{-} > w_{s1}^{+} > \cdots > w_{s\ell}^{-} > w_{s\ell}^{+} > w_{s\ell+1}^{-} \cdots \quad (33)$$

If the angle of incidence w_{so}^{-} of the direct refracted ray is not too close to the angle of total reflection, $\sin^{-1}n$ (which coincides with the branch point singularity in the illustration on page 17), the integrals, Eq. 26, can be approximated by their first-order saddle point contributions, namely,

$$I_{\ell}^{\pm} \sim \frac{2e^{-i\pi/4}}{k_1\rho} \frac{F_{\ell}(w_{s\ell}^{\pm})}{\sqrt{|\ddot{q}_{\ell}^{\pm}(w_{s\ell}^{\pm})|}} e^{ik_1\rho q_{\ell}^{\pm}(w_{s\ell}^{\pm})}, \quad (34)$$

$$k_1\rho \sim \infty$$

where $\ddot{q}_{\ell}^{\pm}(w_{s\ell}^{\pm})$ is the second derivative of Eq. 24, evaluated at the appropriate saddle point. When the observation point is sufficiently close to the interface, or if $\rho \gg h$, w_{so}^{-} will approach the angle of total reflection. In this case, one or more saddle points will lie near the branch point, necessitating a more elaborate asymptotic evaluation of $I_{\ell}^{\pm}$. The result is that the geometrical acoustics ray description must be supplemented to include diffraction effects in the form of lateral waves (Ref. 2).

Eq. 34 can be written explicitly in terms of ray path lengths and ray tube cross sections. Denote by $R_{\ell}^{\pm}$ the path traversed by an incident ray in medium 1 and by $S_{\ell}^{\pm}$ the total path length of a multiply reflected ray in medium 2. Referring to the geometry of the illustration on page 21, one has for the total phase in medium 1,

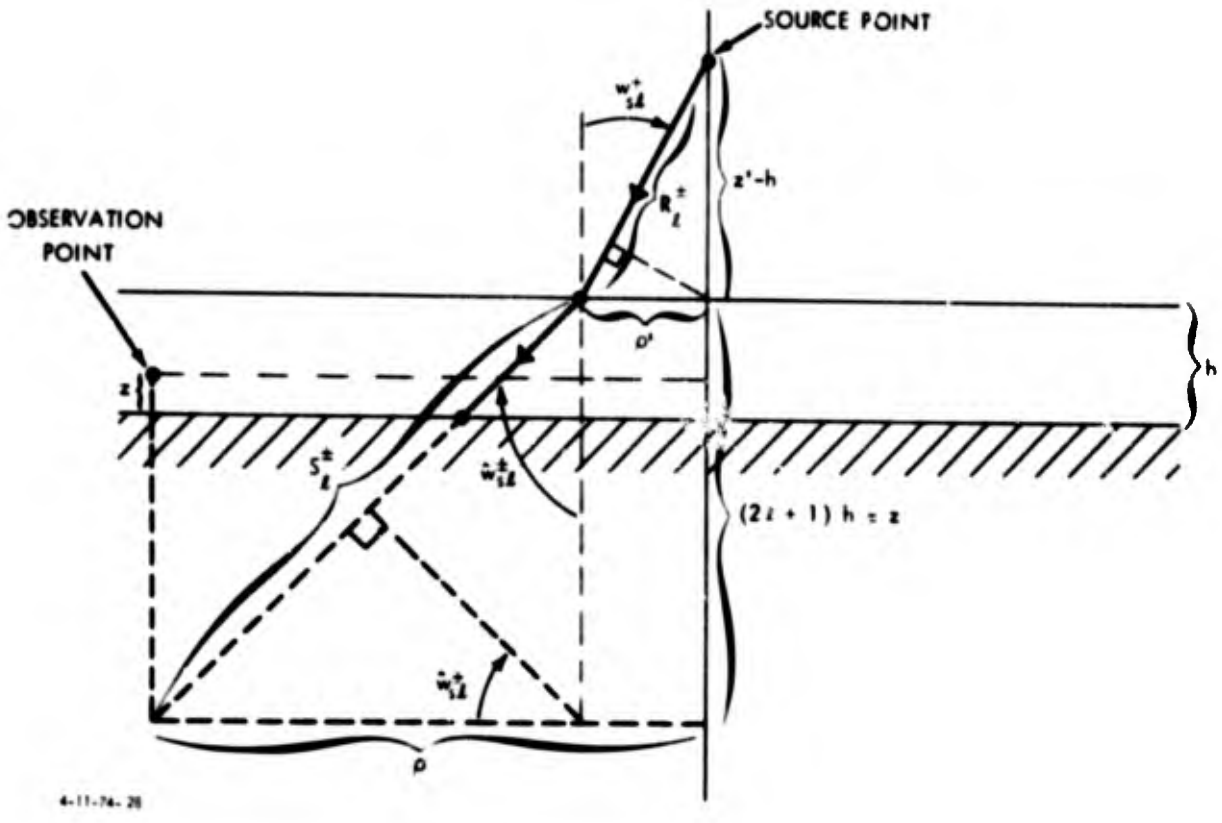

$$k_1 R_\ell^{\pm} = k_1 \rho' \sin w_{s\ell}^{\pm} + k_1 (z'-h) \cos w_{s\ell}^{\pm}, \tag{35}$$

while for the total phase in medium 2, one obtains

$$k_2 S_\ell^{\pm} = k_2 (\rho-\rho') \sin \hat{w}_{s\ell}^{\pm} + k_2 [(2\ell+1) h \pm z] \cos \hat{w}_{s\ell}^{\pm} . \tag{36}$$

Adding Eqs. 35 and 36, and taking account of Snell's law, i.e.,

$k_1 \sin w_{s\ell}^{\pm} = k_2 \sin \hat{w}_{s\ell}^{\pm}$, yields

$$k_1 R_\ell^{\pm} + k_2 S_\ell^{\pm} = k_1 \rho \sin w_{s\ell}^{\pm} + k_1 (z'-h) \cos w_{s\ell}^{\pm} \tag{37}$$

$$+ k_1 [(2\ell + 1)h \pm z] \sqrt{n^2 - \sin^2 w_{s\ell}^{\pm}} .$$

Comparing this with Eq. 24, one identifies the exponential term in Eq. 34 with the total phase change along the ray paths, namely,

$$k_1 \rho\, q_\ell^{\pm}(w_{s\ell}^{\pm}) = k_1 R_\ell^{\pm} + k_2 S_\ell^{\pm} . \tag{38}$$

The ray amplitude factor in Eq. 34 can also be expressed in terms of $R_\ell^{\pm}$ and $S_\ell^{\pm}$. Differentiating Eq. 30 yields

$$\ddot{q}_\ell^{\pm}(w) = -\sin w - \left(\frac{z'-h}{\rho}\right)\cos w - \frac{(2\ell+1)h \pm z}{\rho}\left\{\frac{\cos^2 w - \sin^2 w}{\sqrt{n^2 - \sin^2 w}} + \frac{\sin^2 w \cos^2 w}{(n^2 - \sin^2 w)^{3/2}}\right\} . \tag{39}$$

After evaluating the preceding expression at $w = w_{s\ell}^{\pm}$ and employing Snell's law, the result can be written in the following form:

$$\ddot{q}_\ell^{(\pm)}(w_{s\ell}^{\pm}) = \sin w_{s\ell}^{\pm} - \left(\frac{z'-h}{\rho}\right)\cos w_{s\ell}^{\pm} + \frac{\sin^2 w_{s\ell}^{\pm}}{n \cos \hat{w}_{s\ell}^{\pm}}\left\{\frac{(2\ell+1)h \pm z}{\rho}\right\} - \frac{\cos^2 w_{s\ell}^{\pm}}{n \cos^2 \hat{w}_{s\ell}^{\pm}}\left\{\frac{(2\ell+1)h \pm z}{\rho}\right\} . \tag{40}$$

From the illustration on page 21, one obtains

$$(2\ell+1)h \pm z = S_\ell^{\pm} \cos w_{s\ell}^{\pm} , \tag{41}$$

and

$$\frac{\sin^2 w_{s\ell}^{\pm}}{n} S_\ell^{\pm} = n\, S_\ell^{\pm} \sin^2 \hat{w}_{s\ell}^{\pm} = S_\ell^{\pm} \sin w_{s\ell}^{\pm} \sin \hat{w}_{s\ell}^{\pm} \tag{42}$$

$$= (\rho - \rho') \sin w_{s\ell}^{\pm} .$$

After substituting Eq. 41 and Eq. 42 into Eq. 40, and taking account of Eq. 35, the final version of Eq. 40 reads:

$$\frac{\rho\, \ddot{q}_\ell^{(\pm)}\left(w_{s\ell}^{\pm}\right)}{k_1} = -\cos^2\left(w_{s\ell}^{\pm}\right)\left[\frac{R_\ell^{\pm}}{k_1\cos^2 w_{s\ell}^{\pm}} + \frac{S_\ell^{\pm}}{k_2\cos^2 \hat{w}_{s\ell}^{\pm}}\right]. \quad (43)$$

With the aid of Eqs. 38 and 43, the amplitude and phase of a typical ray in Eq. 34 are given by

$$I_\ell^{\pm} \sim \frac{2e^{-i\pi/4}}{k_1\sqrt{\rho}}\, \frac{F_\ell\left(w_{s\ell}^{\pm}\right)}{\cos w_{s\ell}^{\pm}}\, \frac{e^{i\left[k_1 R_\ell^{\pm} + k_2 S_\ell^{\pm}\right]}}{\left[\frac{R_\ell^{\pm}}{k_1\cos^2 w_{s\ell}^{\pm}} + \frac{S_\ell^{x}}{k_2\cos^2 \hat{w}_{s\ell}^{\pm}}\right]^{\frac{1}{2}}}, \quad (44)$$

$$k_1\rho \sim \infty$$

and the complete geometrical acoustics ray series follows from Eqs. 25 and 26:

$$\Psi(\rho,z) \sim \frac{mk_1}{2\pi\sqrt{k_1\rho}} \quad (45)$$

$$k_1\rho \sim \infty$$

$$\sum_{\ell=0}^{\infty} \sqrt{\sin w_{s\ell}^{\pm}}\, \frac{\left(k_1\cos w_{s\ell}^{\pm} - m\, k_2\cos \hat{w}_{s\ell}^{\pm}\right)^{\ell}}{\left(k_1\cos w_{s\ell}^{\pm} + m\, k_2\cos \hat{w}_{s\ell}^{\pm}\right)^{\ell+1}}\, \frac{e^{i\left[k_1 R_\ell^{\pm} + k_2 S_\ell^{\pm}\right]}}{\left[\frac{R_\ell^{\pm}}{k_1\cos^2 w_{s\ell}^{\pm}} + \frac{S_\ell^{\pm}}{k_2\cos^2 \hat{w}_{s\ell}^{\pm}}\right]^{\frac{1}{2}}}.$$

As mentioned in the preceding, the ray series is valid for $k_1\rho \gg 1$, $k_1(z'-h) \gg 1$ and ρ comparable in magnitude to h-z, i.e., $w_{s\ell}^{\pm}$ not near the angle of total reflection. From Eq. 45 one notes that as the angle of total reflection is approached, $\cos \hat{w}_{s\ell} \to 0$, and the ray amplitudes tend to zero. This result is, of course, factitious and a more accurate asymptotic evaluation would exhibit nonzero values in terms of lateral waves. It is true, however, that near $\hat{w}_{s\ell}^{\pm} \approx \pi/2$ the ray tube cross sections in medium 2 increase, thus implying a reduction in power density. Moreover, the lateral wave contribution

decays more rapidly with $h k_1 \rho$ than the terms in the geometrical acoustics series. To obtain a representation of the acoustic potential valid for large ρ with $\rho >> (h-z)$, one could employ an asymptotic evaluation which includes lateral waves. However, the resulting series, just as the ray series in Eq. 45, converges very slowly, particularly for small m.

A more rapidly convergent representation for the acoustic potential at great distances from the source is afforded by a residue series of leaky waves. Such a series can be obtained directly from the ray series with the aid of the Poisson transformation (see Ref. 3). It is more instructive, however, to proceed directly from the integral representation, Eq. 21. Rather than expand T(w) in the geometric series in Eq. 22, an asymptotic evaluation involving the closed form of the integrand will be effected. As a preliminary step, it is desirable to express the relative location of the source and observation points in terms of new variables shown in the following sketch.

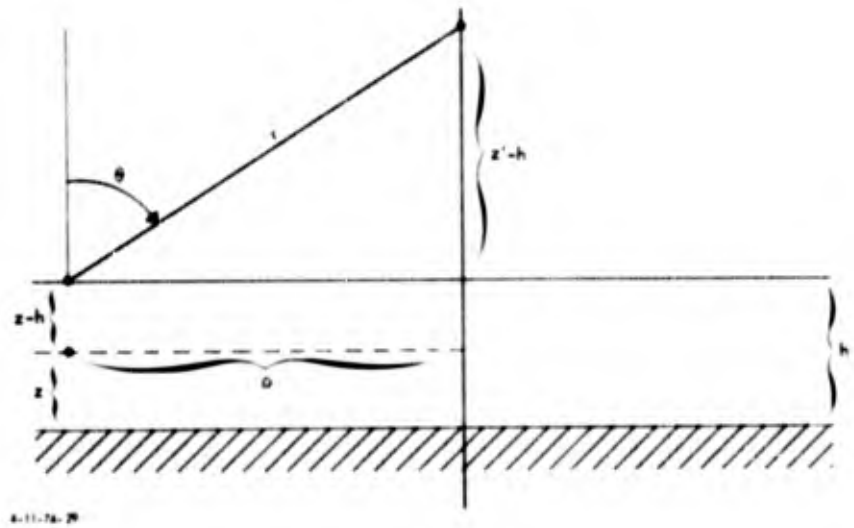

With reference to the sketch above, one has

$$\rho = r \sin \vartheta \ , \ z' - h = r \cos \vartheta \ ,$$

and Eq. 21 is written

$$\Psi = \frac{imk_1^2}{4\pi}\sqrt{\frac{2}{\pi k_1 \rho}}\, e^{-i\pi/4}\int_P \sqrt{\sin w}\,\cos w\, T(w)\, e^{ik_1 r\cos(w-\theta)}\, dw\ . \qquad (46)$$

The integral is taken over the path P in the sketch on page 14. It can be evaluated for large $k_1 r$ by deforming P into the steepest-descents path (SDP) passing through the saddle point $w = \theta$, as shown in the following illustration.

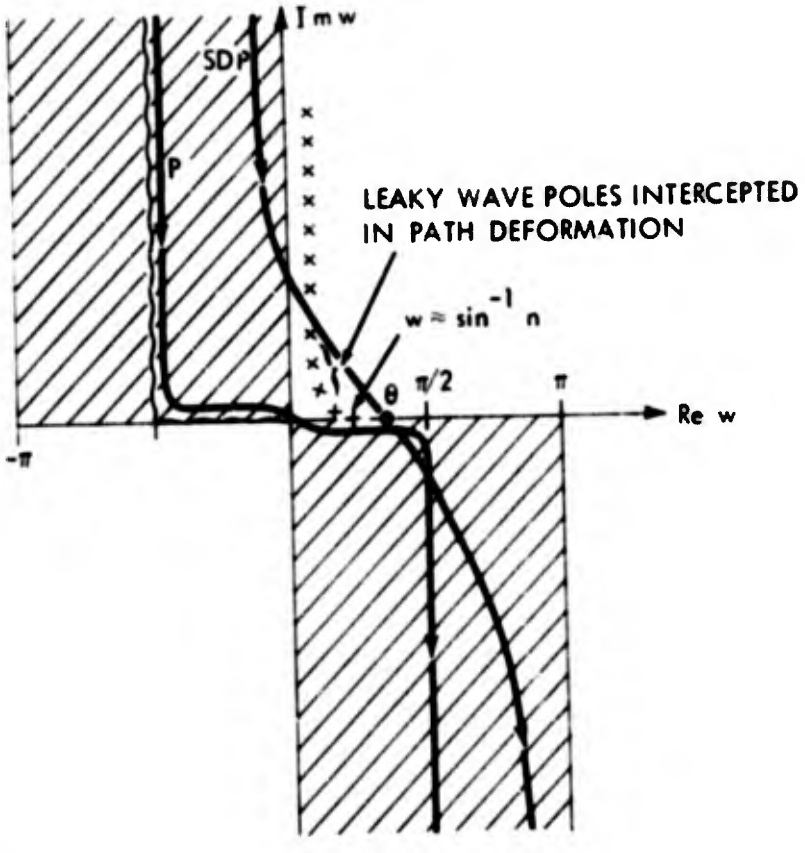

4-11-74-30

In deforming P into SDP, a number of poles will be intercepted. Consequently, Ψ will be represented as a series, corresponding to the residues at these poles, plus an integral to be evaluated asymptotically at the saddle point $w = \theta$. As stated in the preceding, the

location of these poles is determined from the solution of the secular equation (Eq. 16). Taking account of the transformation $K = \kappa_1 \sin w$, Eq. 16 is equivalent to two simultaneous equations:

$$\kappa_1 h \cot \kappa_2 h = im\kappa_2 h \ , \tag{47a}$$

$$\kappa_2^2 - \kappa_1^2 = k_1^2(n^2 - 1) \ , \tag{47b}$$

where $\kappa_1 = k_1 \cos w_\ell$, $\kappa_2 = k_1\sqrt{n^2 - \sin^2 w_\ell}$, and w_ℓ denotes a typical pole location in the w-plane. As in the case of the geometrical acoustics ray series, it will be assumed that $n < 1$ and $m << 1$. From Eq. 47, one can readily establish that the first of these constraints precludes the existence of solutions for which κ_1 is purely imaginary. Such solutions would correspond to surface waves, having pole locations as indicated in the illustration on page 14. Thus, in the deformation of the integration path into the path of steepest descents in the sketch on page 25, only leaky wave poles will be intercepted. The pertinent leaky wave poles are located in the region of the w-plane defined by $0 < \text{Re } w < \pi/2$, $\text{Im } w > 0$. For the case $m << 1$, the leaky wave pole locations can be solved for from Eq. 47 by a perturbation technique. The zeroth order pole locations are determined by setting $m = 0$. This corresponds to a perfectly reflecting boundary at $z = h$, leading to an infinite set of characteristic wavenumbers for a lossless parallel plate wave guide of height h. With $m = 0$, the zeroth order solutions of Eq. 47a are

$$\kappa_{2\ell}^{(0)} = \left(\frac{2\ell+1}{h}\right)\frac{\pi}{2}, \quad \ell = 0, 1, 2, \ldots , \tag{48}$$

or, expressed in terms of w_ℓ, one has

$$k_1 \sin w_\ell^{(0)} = k_1\sqrt{n^2 - \left(\frac{(2\ell + 1)\pi}{2k_1 h}\right)^2} \ . \tag{49}$$

The preceding can be interpreted as the propagation constant in the ρ direction of a typical wave guide mode. For

$$n > \frac{(2\ell + 1)}{2k_1 h} \tag{50}$$

$\sin w_\ell^{(0)}$ is purely real, the wave guide modes propagate without attenuation, and the poles are located on the segment of the real w axis defined by $0 < \mathrm{Re}\ w_\ell < \sin^{-1} n$. When

$$n < \frac{(2\ell + 1)\pi}{2k_1 h}\ , \tag{51}$$

$\sin w_\ell^{(0)}$ is purely imaginary, the wave guide modes attenuate in the ρ direction, and the corresponding poles lie on the positive branch of the imaginary w axis. To obtain approximate solutions for the pole locations when $m \neq 0$, one first eliminates $\varkappa_1$ in Eq. 47, with the result

$$\cot \varkappa_2 h = im \frac{\varkappa_2 h}{\sqrt{(\varkappa_2 h)^2 + (1 - n^2)(k_1 h)^2}}\ ,$$

which may also be expressed in the alternate form

$$-e^{2i\varkappa_2 h} = 1 + m \frac{(\varkappa_2 h)\left(1 - e^{2i\varkappa_2 h}\right)}{\sqrt{(\varkappa_2 h)^2 + (1-n^2)(k_1 h)^2}}\ . \tag{52}$$

The solution for $\varkappa_2 h$ is now written as the sum of its zeroth order value, Eq. 48, and a small increment δ_ℓ (which depends on m):

$$\varkappa_{2\ell} h = \frac{(2\ell+1)\pi}{2} + \delta_\ell\ ,\ \ell = 0, 1, 2, \ldots . \tag{53}$$

Substituting Eq. 53 into Eq. 52, yields

$$\delta_\ell = -\frac{1}{2} \ln \left[1 + m \frac{\left(\frac{(2\ell+1)\pi}{2} + \delta_\ell\right) \left(1 + e^{2i\delta_\ell}\right)}{\sqrt{\left[\frac{(2\ell+1)\pi}{2} + \delta_\ell\right]^2 + (1-n^2)(k_1 h)^2}} \right] . \qquad (54)$$

For small m, Eq. 54 can be solved for δ_ℓ by a series of successive iterations, since a small m corresponds to δ_ℓ of the same order of magnitude. Thus, substitution of the k-th order value of δ_ℓ on the right side of Eq. 54 yields, on the left side, the k+1-th order value. In particular, to the first-order approximation,

$$\delta_\ell \approx -\, im \frac{(2\ell+1)\pi/2}{\sqrt{\left[\frac{(2\ell+1)\pi}{2}\right]^2 + (1-n^2)(k_1 h)^2}} , \quad \ell = 0, 1, 2, \ldots , \qquad (55)$$

which follows from Eq. 54 with the aid of $\ell n(1 + \Delta x) \approx \Delta x$, valid for $\Delta x \ll 1$. Once the solution for δ_ℓ has been obtained, the location of the poles in the w-plane is determined from

$$\sin w_\ell = \sqrt{n^2 - \left[\frac{(2\ell+1)\pi + \delta}{2hk_1}\right]^2} , \qquad (56a)$$

$$\cos w_\ell = \sqrt{1 - n^2 + \left[\frac{(2\ell+1)\pi + \delta}{2hk_1}\right]^2} . \qquad (56b)$$

Since $\delta_\ell \ll 1$, the leaky wave poles corresponding to "propagating" modes, that is, in the region $0 < \text{Re } w_\ell < \sin^{-1} n$, are displaced slightly above the real w axis, while those for the evanescent modes are shifted by a small amount to the right of the imaginary w-axis. No pole singularities exist with $\text{Re } w_\ell > \sin^{-1} n$, which is the angle of total reflection. From the sketch on page 24 one notes that for observation points sufficiently far removed from the source point, $\theta \to \pi/2$. Thus, the saddle point $w_s = \theta$ (see sketch on page 25) will lie to the right of

the angle of total reflection, and for $n^2 \ll 1$, the asymptotic evaluation of the integral along the steepest descents path will be unaffected by pole singularities. Decomposing Ψ in Eq. 46 into a sum comprising the SDP contribution and a leaky wave residue series, one can write

$$\Psi = \Psi_{SDP} + \Psi_{RES} \cdot \tag{57}$$

Focussing first on the SDP contribution, and assuming initially that $\theta < \pi/2$, the first-order saddle point contribution in Eq. 46 is

$$\Psi_{SDP} \sim \cos\theta \frac{mk_1}{2\pi} \frac{e^{ik_1 r}}{r} \tag{58}$$
$$k_1 r \sim \infty$$

$$\frac{\cos\left[k_1 z\sqrt{n^2 - \sin^2\theta}\right]}{k_1 \cos\theta \cos\left[k_1 h\sqrt{n^2 - \sin^2\theta}\right] - im\, k_1\sqrt{n^2 - \sin^2\theta}\, \sin\left[k_1 h\sqrt{n^2 - \sin^2\theta}\right]}$$

Since $\sin\theta > n$, the square roots yield purely imaginary numbers. Consequently, at observation points sufficiently far below the medium interface, Ψ_{SDP} decays exponentially with $(h-z)$. Indeed, if $(h-z)k_1 \gg 1$, Eq. 58 can be approximated by

$$\Psi_{SDP} \sim \cos\theta \frac{m}{2\pi} \frac{e^{ik_1 r}}{r} \frac{e^{-k_1\sqrt{\sin^2\theta - n^2}\,(h-z)}}{\cos\theta + m\sqrt{\sin^2\theta - n^2}} \cdot \tag{59}$$
$$k_1 r \sim \infty$$

Evidently, when $k_1 h \gg 1$, the saddle point contribution does not constitute the dominant portion of the acoustic potential in Eq. 57, except for observation points at or near the medium interface. When $\theta \to \pi/2$, as will necessarily be the case for sufficiently large ρ, the first-order asymptotic term, Eq. 58, tends to zero. In this case, the second term in the asymptotic series for large $k_1 r$ dominates. One can show that at $\theta = \pi/2$ this dominant term is

$$\Psi_{SDP} \sim \frac{3}{2\pi}\left(\frac{h}{m}\right)\frac{e^{ik_1\rho}}{\sqrt{1-n^2\rho^2}}\coth\left[k_1h\sqrt{1-n^2}\right]\frac{\cosh\left[k_1z\sqrt{1-n^2}\right]}{\sinh\left[k_1h\sqrt{1-n^2}\right]} \quad . \qquad (60)$$

$k_1\rho \sim \infty$

At the interface z=h, assuming $k_1h\sqrt{1-n^2} >> 1$,

$$\Psi_{SDP} \sim \frac{3}{2\pi}\,\frac{h}{m\sqrt{1-n^2}}\,\frac{e^{ik_1\rho}}{\rho^2}\,, \qquad (61)$$

whereas below the interface, one again obtains an exponentially decaying result, namely,

$$\Psi_{SDP} \sim \frac{3}{2\pi}\,\frac{h}{m}\,\frac{e^{ik_1\rho}}{\sqrt{1-n^2\,\rho^2}}\,e^{-k_1\sqrt{1-n^2}(h-z)} \quad . \qquad (62)$$

In view of the foregoing comments, the potential function for $\theta > \sin^{-1}n$, $(h-z)\,k_1 >> 1$ and $k_1\rho >> 1$ is determined entirely by a residue series of leaky waves. Upon equating Eq. 46 to $2\pi i$ times the sum of residues enclosed between P and SDP, one obtains, with the aid of Eq. 19,

$$\Psi\,(\rho,z,z') \sim \frac{(2\pi i)imk_1^2}{4\pi}\sqrt{\frac{2}{\pi k_1\rho}} \qquad (63)$$

$k_1\rho \sim \infty$

$$\cdot \sum_{\ell}\sqrt{\sin w_\ell}\,\cos w_\ell\; e^{ik_1 r\cos(w_\ell-\theta)}\;\frac{\cos \varkappa_{2\ell} z}{\frac{d}{dw}\left[k_1\cos w\cos\varkappa_2 h - im\varkappa_2\sin\varkappa_2 h\right]_{w=w_\ell}} \quad .$$

Each individual leaky wave mode decays with ρ in accordance with the "cylindrical spreading" factor $1/\sqrt{\rho}$ and, in addition, possesses an exponential dependence on ρ contained in $k_1 r\cos(w_\ell - \theta)$, which may be written

$$k_1 r \cos(w_\ell - \theta) = k_1(z' - h) \cos w_\ell + k_1 \rho \sin w_\ell \ . \qquad (64)$$

In the zeroth order approximation m = 0, Eq. 49, the last term in Eq. 64 is purely real in the propagation region (Eq. 50), and purely (positive) imaginary in the evanescent region (Eq. 51). Because of the exponential attenuation of the evanescent modes with ρ, the sum in Eq. 63 can be truncated to include only the finite number of propagating modes, equal approximately to nk_1h/π. For $m \neq 0$, the boundary between propagating and evanescent modes is no longer sharply defined, a phenomenon similar to that which obtains generally in dissipative media. Even though the media under present consideration are dissipationless, the power carried by a typical mode propagating in the lower medium is attenuated by virtue of its continuous "leakage" across the interface z = h. As a result, $\sin w_\ell$ always has a nonzero imaginary part, resulting in an exponential attenuation of each leaky wave with ρ. However, for small m this exponential decay for modes with $0 \leq \ell \lesssim nk_1h/\pi$ can be quite small, the attenuation of each individual mode with ρ being governed primarily by the cylindrical spreading factor $1/\sqrt{\rho}$. On the other hand, the variation of the total acoustic potential with ρ may exhibit rather complicated oscillatory behavior due to phase interference effects, especially if the number of propagating modes is large.

For $m \ll 1$, $\varkappa_{2\ell}h$ in Eq. 63 can be replaced by its zeroth-order approximation, that is, $\frac{(2\ell + 1)\pi}{2}$, and the term containing m in the denominator may be neglected. With these modifications, Eq. 63 reduces to

$$\Psi(\rho, z, z') \sim \frac{-m}{2k_1h} e^{-i\pi/4} \sqrt{\frac{2}{\pi k_1 \rho}}$$

$$k_1\rho \sim \infty$$

$$\cdot \sum_{\ell=0}^{\infty} (-1)^\ell \frac{(2\ell + 1)}{2h} \frac{\cos\left[\frac{(2\ell+1)\pi z}{2h}\right] e^{ik_1(z'-h)\cos w_\ell}}{\cos w_\ell \sqrt{\sin w_\ell}} e^{ik_1\rho \sin w_\ell} \ . \qquad (65)$$

The number of terms in the series required for convergence is approximately $k_1 hn/\pi$, equal to the number of propagating waves. The roots w_ℓ may be computed by means of the previously described perturbation technique. In the range of ℓ, satisfying

$$1-n^2 \gg \left[\frac{(2\ell+1)\pi}{2k_1 h}\right]^2 , \tag{66}$$

the first-order perturbation parameter δ_ℓ in Eq. 55 may be written

$$\delta_\ell = -\text{im} \frac{(2\ell+1)\pi}{2k_1 h \sqrt{1-n^2}} \tag{67}$$

and, employing Eq. 56,

$$\sin w_\ell \approx \sqrt{n^2 - \left[\frac{(2\ell+1)\pi}{2k_1 h}\right]^2 \left[1 - \frac{\text{im}}{k_1 h \sqrt{1-n^2}}\right]} , \tag{68a}$$

$$\cos w_\ell \approx \sqrt{1 - n^2} . \tag{68b}$$

If the relative refractive index is small, that is, $2n^2 \ll 1$, the range of ℓ where Eq. 66 fails to hold corresponds to evanescent waves. Consequently, Eq. 68 may be employed in Eq. 65 for all ℓ. In view of Eq. 68b, one notes from Eq. 65 that the magnitude of the acoustic potential is only weakly dependent on the height of the source above the interface.

C. ASYMPTOTIC EVALUATION OF ACOUSTIC POTENTIAL FOR A LAYER WITH A LINEARLY VARYING REFRACTIVE INDEX PROFILE

The preceding asymptotic evaluation can also be carried out for a layer with a linearly varying refractive index profile,* defined by

*Actually, $n^2(z) = N^2 - a(h-z)$, that is, the square of the index is linear. However, for $a(h-z)/N^2 \ll 1$, $n(z) \approx 1 - a/2N\ (h-z)$.

Eq. 10. For $a > 0$, the refractive index decreases from N ($N < 1$) just below the interface to $N\sqrt{1 - \frac{ah}{N^2}}$ at the perfectly impenetrable bottom boundary $z = 0$, as shown below.

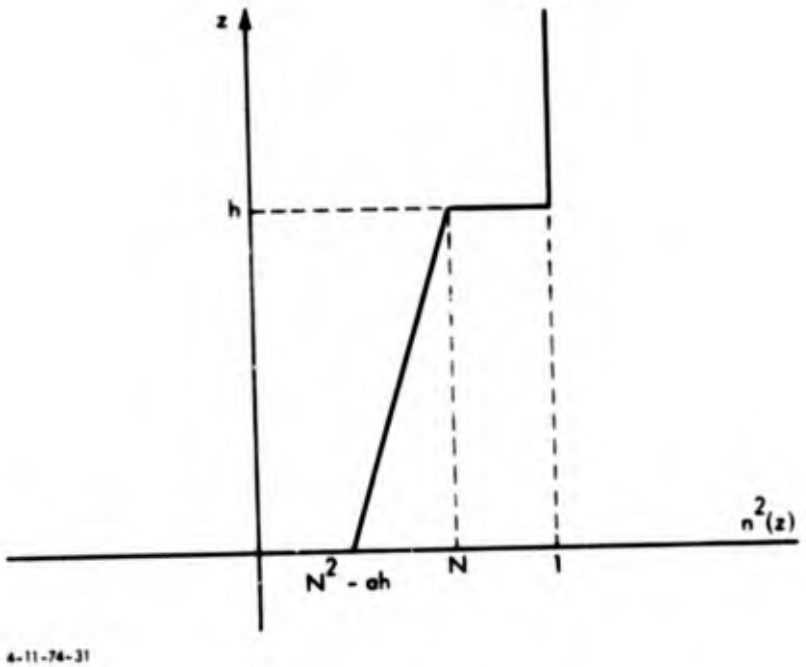

An integral representation for Ψ at observation points within the layer follows from Eq. 4 in conjunction with Eqs. 7, 13, and 14. Following the same procedure as in the case of a constant refractive index, the acoustic potential can be represented as in Eq. 46, the only modification being that $T(w, z)$ must now be replaced by $\hat{T}(w, z)$,

$$\hat{T}(w, z) = \frac{X(w, z)}{k_1 \cos w\, X(w,h) + im\, Y(w)}, \tag{69}$$

where

$$X(w, z) = Ai\left[\left(k_1^2 a\right)^{1/3} z_p\right] Bi\left[\left(k_1^2 a\right)^{1/3} (z_p - z)\right] - Bi\left[\left(k_1^2 a\right)^{1/3} z_p\right] Ai\left[\left(k_1^2 a\right)^{1/3} (z_p - z)\right], \tag{70}$$

$$Y(w) = \left(k_1^2 a\right)^{1/3} \left\{ \dot{A}i\left[\left(k_1^2 a\right)^{1/3} (z_p - h)\right] \dot{B}i\left[\left(k_1^2 a\right)^{1/3} z_p\right] \right. \tag{71}$$

$$\left. - \dot{B}i\left[\left(k_1^2 a\right)^{1/3} (z_p - h)\right] \dot{A}i\left[\left(k_1^2 a\right)^{1/3} z_p\right] \right\} ,$$

and

$$z_p = h - \left(\frac{N^2 - \sin^2 w}{a}\right) . \tag{72}$$

The monotonic variation of n(z) within the layer precludes localized internal ducting of acoustic energy and, since the refractive index of the layer is less than unity, no surface waves can be supported by the interface. Consequently, the nature of the singularities of the integrand and their disposition relative to the path of integration P in the illustration on page 25 will not differ substantially from the situation which obtains in a homogeneous medium, especially if the slope parameter a is small. From considerations quite analogous to those employed in conjunction with the spatially invariant refractive index profile, one finds that the acoustic potential at large radial distances from the source is more readily amenable to numerical computation when expressed as a leaky wave residue series rather than as a ray acoustics series. When the path of integration is deformed from P to SDP, one can again express Ψ for large $k_1 \rho$ ($\theta \rightarrow \pi/2$) as a sum of a saddle point contribution and a leaky wave residue series. For a certain range of parameters the saddle point contribution will be shown to account for a significant portion of the acoustic potential only at observation points very near the interface, being subject to an exponential decay with (h-z) similar to that given by Eqs. 59 and 60. In view of the previous discussion concerning the saddle point contribution in Eq. 58, it is sufficient to show that the integrand, Eq. 46 or, more precisely, $\hat{T}(w,z)$ in Eq. 69, decays exponentially with (h-z) for $\theta = \pi/2$. For this purpose, one can employ the asymptotic

properties of Airy functions for large arguments. Let σ be a real nonnegative parameter. Then for $\sigma \gg 1$, the Airy functions possess the following oscillatory behavior (Ref. 3):

$$\mathrm{Ai}(-\sigma) \sim \frac{1}{\sqrt{\pi}\sigma^{\frac{1}{4}}} \sin\left(\frac{2}{3}\sigma^{3/2} + \pi/4\right), \tag{73a}$$

$$\mathrm{Bi}(-\sigma) \sim \frac{1}{\sqrt{\pi}\sigma^{\frac{1}{4}}} \cos\left(\frac{2}{3}\sigma^{3/2} + \pi/4\right), \tag{73b}$$

$$\dot{\mathrm{A}}\mathrm{i}(-\sigma) \sim -\frac{1}{\sqrt{\pi}}\sigma^{\frac{1}{4}} \cos\left(\frac{2}{3}\sigma^{3/2} + \frac{\pi}{4}\right), \tag{73c}$$

$$\dot{\mathrm{B}}\mathrm{i}(-\sigma) \sim \frac{1}{\sqrt{\pi}}\sigma^{\frac{1}{4}} \sin\left(\frac{2}{3}\sigma^{3/2} + \frac{\pi}{4}\right). \tag{73d}$$

On the other hand, when the arguments are large and positive, the Airy functions behave like growing or decaying exponentials, viz.,

$$\mathrm{Ai}(\sigma) \sim \frac{1}{2\sqrt{\pi}\sigma^{\frac{1}{4}}} e^{-\frac{2}{3}\sigma^{3/2}}, \tag{74a}$$

$$\mathrm{Bi}(\sigma) \sim \frac{1}{\sqrt{\pi}\sigma^{\frac{1}{4}}} e^{\frac{2}{3}\sigma^{3/2}}, \tag{74b}$$

$$\dot{\mathrm{A}}\mathrm{i}(\sigma) \sim -\frac{\sigma^{\frac{1}{4}}}{2\sqrt{\pi}} e^{-\frac{2}{3}\sigma^{3/2}}, \tag{74c}$$

$$\dot{\mathrm{B}}\mathrm{i}(\sigma) \sim \frac{\sigma^{\frac{1}{4}}}{\sqrt{\pi}} e^{\frac{2}{3}\sigma^{3/2}}. \tag{74d}$$

The asymptotic forms, Eq. 74, may be employed in Eqs. 70 and 71 if all the arguments in the Airy functions are large and positive. With $w = \theta = \pi/2$, this will be the case if

$$(k_1 a)^{1/3} \left[\left(\frac{1-N^2}{a}\right) + h-z\right] \gg 1 , \tag{75}$$

or, since $h-z \geq 0$, it is sufficient to require

$$1-N^2 \gg k_1^{1/3} \left(\frac{a}{k_1}\right)^{2/3} , \tag{76}$$

which can be satisfied for sufficiently large k_1 or sufficiently small a. The maximum permissible value of a is N^2/h, since it reduces the refractive index at $z = 0$ to zero. Consequently, a sufficient condition ensuring Eq. 76 is

$$1-N^2 \gg N \frac{(k_1 N)^{1/3}}{(k_1 h)^{2/3}} , \tag{77}$$

and can be satisfied if the layer depth h is large in terms of wavelengths. Assuming this to be the case, one can readily establish with the aid of Eq. 74 that $\hat{T}(\pi/2,z)$ decays exponentially below the interface and, consequently, that the saddle point contribution to the total acoustic potential for $k_1(h-z) > 0$ is negligibly small. The dominant contribution arises from the leaky wave series, which may be written (for $k_1\rho \sim \infty$ and $k_1(h-z) \gg 1$)

$$\Psi(\rho,z,z') \sim \frac{(2\pi i)\ imk_1^2}{4\pi} \sqrt{\frac{2}{\pi k_1 \rho}}\, e^{-i\pi/4} \tag{78}$$

$$\cdot \sum_{\ell} \sqrt{\sin w_\ell}\, \cos w_\ell\, e^{ik_1 r \cos(w_\ell - \theta)} \frac{X(w_\ell, z)}{\frac{d}{dw}\left[k_1 \cos w\, X(w,h) + im\, Y(w)\right]_{w = w_\ell}} ,$$

where the leaky wave poles, w_ℓ, are determined from the solution of

$$k_1 \cos w_\ell\, X(w_\ell, h) + im\, Y(w_\ell) = 0 . \tag{79}$$

The general form of the result (Eq. 78) is very similar to the leaky wave series for the constant refractive index profile, Eq. 63, and the qualitative comments regarding the physical interpretation of leaky waves, and convergence properties of the series made in conjunction with Eq. 63 are also applicable to Eq. 78. As in the constant refractive index case, the solution of the secular equation for small m can be effected with the aid of a perturbation technique for which the zeroth-order solutions correspond to the roots of

$$X(w_\ell, h) = 0 \ . \tag{80}$$

Evidently, as the slope parameter (a) tends to zero, Eq. 78 must approach Eq. 63. It is of interest to inquire how small (a) must be in order that Eq. 63 constitute an acceptable approximation in a layer with a linearly varying refractive index profile. The transition from Eq. 78 to Eq. 63 follows upon recognizing that for $\sin w \neq N$ and sufficiently small a, the resulting large arguments of the Airy functions permit their replacement by first-order asymptotic forms. Substitution of these asymptotic forms in Eq. 78 yields Eq. 63. In examining Eq. 78 for small a, only those values of w lying near the leaky wave poles need be considered. In particular, if $m \ll 1$, only the region $0 \leq \sin w < N$ on the real w axis is of interest. In this range of w and for sufficiently small a, the arguments of the Airy function will be negative. Thus if

$$(z-z_p)\left(k_1^2 a\right)^{1/3} \gg 1 \ , \tag{81}$$

the oscillatory asymptotic representations (Eq. 73) are appropriate. Taking account of Eq. 72, Eq. 81 may be written in the following form:

$$N^2 - \sin^2 w_\ell \gg (h-z)\, a + \left(\frac{a}{k_1}\right)^{2/3} \ . \tag{82}$$

Since this inequality must hold for $0 \le z \le h$, increasing h constrains the slope parameters to take on progressively smaller values. If h is sufficiently large, even a very gradual decrease in the refractive index with depth can result in significant deviations of the characteristics of leaky wave mode functions from those computed on the basis of a constant refractive index model. Also, the effect of the approximation is not uniform in w_ℓ, becoming progressively poorer as w_ℓ approaches the angle of total reflection, i.e., $\sin w_\ell \to N$. Consequently, leaky wave poles lying close to $\sin^{-1} N$ will be more sensitive to changes in the slope parameter than those further removed. When $a = 0$ and $m \ll 1$, $\sin w_\ell$ may be approximated by Eq. 49, which, together with Eq. 81, yields

$$(2\ell + 1) \gg \frac{2k_1 h}{\pi} \left[(h-z)\, a + \left(\frac{a}{k_1}\right)^{2/3}\right]^{1/2} . \qquad (83)$$

If Eq. 83 is satisfied for all ℓ, the effect of the variation in refractive index can be neglected, and Eq. 78 may be replaced by Eq. 63. Clearly, as (a) is increased from zero, Eq. 83 will first be violated for the lowest order modes, which are precisely the ones whose poles lie close to the angle of total reflection. These modes correspond to rays with turning points at or above the bottom boundary ($z = 0$). Thus, given an arbitrarily small slope parameter, one can always increase h sufficiently so that one or more rays turn around before reaching the bottom boundary. This interpretation is consistent with Eq. 83, which can be violated for arbitrarily small (a) by increasing h.

In assessing the importance of the magnitude of the slope parameter on the leaky wave series, one should bear in mind that Eq. 83 may fail to hold for only a small number of lowest order modes. As long as these constitute only a small fraction of the total number of propagating modes, the effects of the refractive index inhomogeneity may still be negligible on the overall modal sum.

D. ACOUSTIC POTENTIAL IN A LAYER WITH A HIGHLY ABSORBENT LOWER BOUNDARY

The planar layer with a perfectly rigid boundary at $z = 0$ constitutes a suitable model for physical situations in which the lower boundary is strongly reflecting, i.e., its reflection coefficient is close to unity. In many physical problems, the layer is bounded by a highly absorbent rather than a highly reflecting surface. This absorption may arise from a dissipation mechanism directly associated with the surface constitutive parameters, or it may be the result of random scattering by a highly irregular surface contour. In the latter instance, the scattered acoustic radiation would be largely diffuse and, consequently, could not contribute to constructive reinforcement with a coherent acoustic wave complex. Thus, as concerns the coherent part of the acoustic potential, the energy scattered by the lower boundary may be treated as having been effectively dissipated.

A variety of simplified models can be employed to characterize an acoustically absorbent surface. One analytically tractable model employs a homogeneous (Leontovich type) boundary condition to yield a constant resistive surface impedence. The result of interaction of an incident plane wave with such a constant resistance surface yields a scattered plane wave whose amplitude varies with the angle of incidence. Consequently, perfect absorption is possible for only one direction of incidence. The model postulated herein is that of a "perfectly" absorbent surface, that is, a surface which completely absorbs all incident plane waves <u>irrespective</u> of their angles of incidence. Aside from affording a somewhat greater degree of simplification from the analytical standpoint, a perfect absorber of this type appears to conform more closely to the situation which obtains in the case of an irregularly contoured dissipative surface than does a constant resistance model.

In a layer having a constant refractive index, an ideal planar absorber at $z = 0$ permits only the direct refracted ray to reach the observation point, precisely as is the case for a layer occupying the

entire half space $z < h$. At observation points far removed from the source point and $\rho >> h$, but well below the upper medium interface, the acoustic potential is governed primarily by the second-order geometrical acoustics result obeying the spreading law $1/\rho^2$ (Ref. 2), as contrasted with the cylindrical spreading $1/\sqrt{\rho}$, governing the leaky wave representation in the presence of a perfectly reflecting boundary. Thus, for a constant refractive index profile and large ρ, the presence of a perfectly reflecting surface at $z = 0$ leads to a substantial reinforcement of acoustic potential over that obtained with a perfectly absorbent lower boundary. In this regard, the situation differs drastically from that which obtains in a layer with a linearly decreasing refractive index profile. For, in this case, the rays follow curved trajectories [for sufficiently small (a), these may be approximated by semicircular arcs (Ref. 2)], and consequently, acoustic energy can be "guided" along the interface by virtue of ray reflections taking place at ray caustics rather than at the lower layer boundary. As will be shown in Chapter III, the overall effect of these reflections leads to an average decay given by $1/\sqrt{\rho}$. Various possible ray trajectories are depicted below.

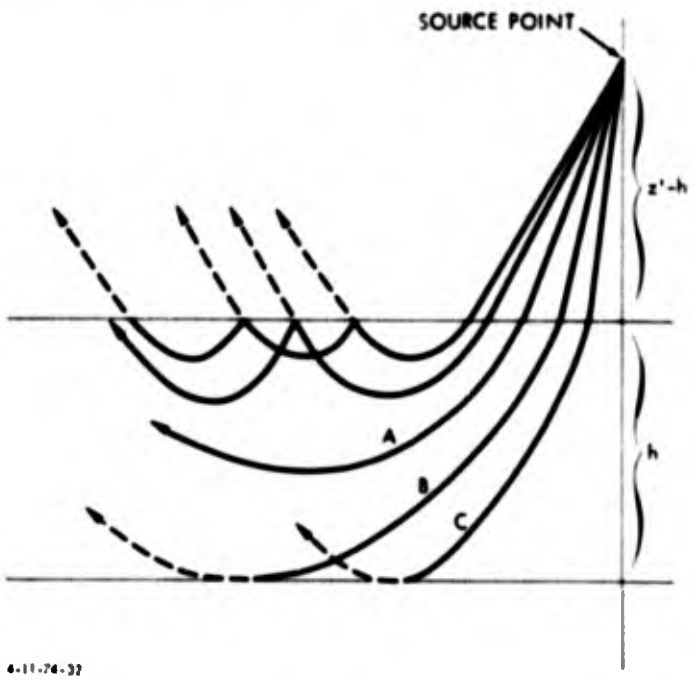

The rays are seen to be of three types: those with turning points above the lower layer boundary (A), those reflected from the lower boundary (C), and the transitional glancing ray (B), whose turning point lies just at the lower boundary. A perfect absorber, as postulated in the preceding, completely suppresses reflections of rays (B) and (C), leaving type (A) rays unaffected. By virtue of multiple reflections at the upper layer boundary, these rays facilitate guiding of acoustic energy with low attenuation, a propagation phenomenon exploited in connection with long-range acoustic detection systems known as SOFAR (Ref. 2). A geometrical acoustics ray description can be employed to show that such multiply reflected rays produce high energy concentrations near the upper layer interface, a wave phenomenon with a direct counterpart in the Whispering Gallery Effect (Refs. 2 and 3) associated with concentration of acoustic energy near concave surfaces with large radii of curvature. In the present application the observation points of interest are far from the upper layer boundary and very near the lower boundary. Since this region corresponds to turning points of one or more rays, the ray description has here only qualitative validity. Moreover, the transition between the critical ray (B) interacting with the ideal absorbing surface and a ray with a turning point just above the lower boundary cannot be examined quantitatively on the basis of geometrical acoustics. Although the ray description can be supplemented by the inclusion of appropriate transition functions yielding correct diffraction effects in regions close to ray turning points, an alternate, and substantially equivalent, representation may be obtained with the aid of the residue series, Eq. 78. This residue series is valid for a perfectly reflecting boundary and, consequently, contains mode functions corresponding to the ray classification in the preceding sketch. Characteristic wave numbers of modes descriptive of propagation properties of type (A) rays will be weakly dependent on h. In particular, if h is chosen sufficiently large, these mode wave numbers should tend to exhibit progressively weaker dependence on h. Therefore, to obtain a mode series appropriate to a layer with a linearly varying profile and a perfectly

absorbent lower boundary, the expressions for the mode functions and characteristic wave numbers in Eq. 78 should be examined for large h, thereby affording their separation from those terms in the series with a strong dependence on the reflecting properties of the lower boundary. The latter part of the series must, perforce, correspond to rays undergoing reflection at z = 0.

As mentioned in conjunction with Eq. 79, for small m, the leaky wave poles corresponding to propagating modes fall approximately on the segment $0 < \sin w < N$ of the real w axis. Hence, in the region of interest $N^2 - \sin^2 w$ is nonnegative. Consider h sufficiently large, such that for all pertinent w

$$\left(k_1^2 a\right)^{1/3} z_p = \left(k_1^2 a\right)^{1/3} \left[h - \frac{N^2 - \sin^2 w}{a}\right] >> 1 \ . \tag{84}$$

The Airy functions in Eqs. 70 and 71 with arguments $\left(k_1^2 a\right)^{1/3} z_p$ may now be replaced by appropriate asymptotic forms. Since z_p is positive, these are given by Eq. 74. In particular, one notes that $\dot{A}i\left[\left(k_1^2 a\right)^{1/3} z_p\right]$ decays, whereas $\dot{B}i\left[\left(h_1^2 a\right)^{1/3} z_p\right]$ increases exponentially. Consequently, for large z_p the terms in Eqs. 70 and 71 containing $\dot{A}i\left[\left(k_1^2 a\right)^{1/3} z_p\right]$ as a factor will be exponentially small and may therefore be deleted. Of course, this deletion is permissible only if the functions containing $z_p - z$ and $z_p - h$ are not themselves of exponential growth, a condition ensured by restricting z to values satisfying $z_p - z < 0$, since for real negative arguments all Airy functions exhibit bounded oscillatory behavior. After eliding the exponentially small terms in Eqs. 70 and 71, T(w,z) in Eq. 69 may be written

$$\hat{T}(w,z) = \frac{Ai\left[\left(k_1^2 a\right)^{1/3} (z_p - z)\right]}{k_1 \cos w \, Ai\left[-\left(\frac{k_1}{a}\right)^{2/3} (N^2 - \sin^2 w)\right] - im\left(k_1^2 a\right)^{1/3} \dot{A}i\left[-\left(\frac{k_1}{a}\right)^{2/3} (N^2 - \sin^2 w)\right]} \ . \tag{85}$$

Equation 85 can be used to generate a residue series analogous to Eq. 78, with the secular equation for w_ℓ now given by

$$0 = k_1 \cos w_\ell \mathrm{Ai}\left[-\left(\frac{k_1}{a}\right)^{2/3}\left(N^2 - \sin^2 w_\ell\right)\right] - im\left(k_1^2 a\right)^{1/3} \dot{\mathrm{A}}\mathrm{i}\left[-\left(\frac{k_1}{a}\right)^{2/3}\left(N^2 - \sin^2 w_\ell\right)\right] \quad (86)$$

The roots w_ℓ are independent of h and infinite in number. Indeed, Eq. 85 is precisely the result that would have been obtained from a direct solution of the problem for a layer with no lower boundary, that is, a refractive index profile having the functional form of Eq. 10 for $-\infty < z < h$. A residue series for a layer with a perfectly absorbent lower boundary may be constructed by retaining only those terms for which $\mathrm{Ai}\left[\left(k_1^2 a\right)^{1/3}(z_p - z)\right]$ decreases monotonically in the region $z < 0$, and possesses oscillatory behavior when $z > 0$. For sufficiently small m, only the zeroth-order approximation

$$\hat{T}(w_1 z) = \frac{\mathrm{Ai}\left[\left(k_1^2 a\right)^{1/3}\left(z_p - z\right)\right]}{k_1 \cos w \, \mathrm{Ai}\left[-\left(\frac{k_1}{a}\right)^{2/3}\left(N^2 - \sin^2 w\right)\right]}, \quad (87)$$

and the associated secular equation is

$$\mathrm{Ai}\left[-\left(\frac{k_1}{a}\right)^{2/3}\left(N^2 - \sin^2 w_\ell\right)\right] = 0 \quad (88)$$

Note that the cosw factor present in Eq. 86 has been omitted in Eq. 88, since it cancels against cosw present in the numerator of the final integral representation, Eq. 46. The zeros of $\mathrm{Ai}(-\sigma)$ have been tabulated (Ref. 4). With the notation

$$\mathrm{Ai}\left(-\sigma_\ell\right) = 0 , \quad (89)$$

the σ_ℓ are all real, nonnegative, and can be arranged in a sequence

$$0 < \sigma_1 < \sigma_2 < \sigma_3 < \ldots . \tag{90}$$

Writing sin w_ℓ in Eq. 88 explicitly in terms of σ_ℓ, one has

$$\sin w_\ell = \left[N^2 - \sigma_\ell \left(\frac{a}{k_1}\right)^{2/3}\right]^{1/2} \quad \ell = 1, 2, 3, \ldots , \tag{91}$$

where, in consonance with previous results, the positive imaginary part of sinw_ℓ is to be chosen if the radicand should become negative. Although Eq. 89 holds for an infinite number of σ_ℓ, only a finite number of these need be retained for a perfectly absorbent lower layer, namely, those which locate the point of transition (that is, the ray turning points) of the Airy function in the numerator of Eq. 87 above the plane z = 0. Expressing the numerator of $\hat{T}(w,z)$ explicitly in terms of σ_ℓ, one obtains

$$\mathrm{Ai}\left[\left(k_1^2 a\right)^{1/3} (z_p - z)\right] = \mathrm{Ai}\left[\left(k_1^2 a\right)^{1/3} (h - z) - \sigma_\ell\right] . \tag{92}$$

Let z_L, $0 < z_L < h$, be the transition point between the ranges of z corresponding to monotonically decaying and oscillating behaviors of Eq. 92 for $\ell = L$. Then,

$$z_L = h - \sigma_L \left(k_1^2 a\right)^{-1/3} , \tag{93}$$

and transition points z_ℓ for $1 \le \ell < L$ all lie above z_L, viz., $z_L < z_\ell$. By virtue of the ordering of roots, Eq. 90, in the range $0 < z < z_L$ Eq. 92 represents a monotonically decreasing function for all $\ell \le L$. This range of z is the shadow side of ray caustics associated with mode indexes $\ell \le L$. On the other hand, when $\ell > L$, the transition points z_ℓ move below the plane $z = z_L$, and oscillatory behavior now penetrates to $z_\ell < z < h$. Hence, if the postulated ideal absorber is placed at z = 0 "just below" z_L, modes with indexes $\ell > L$

can be assumed suppressed and, consequently, discarded in the final residue series summation. The proximity of such an absorber to z_L entails considerable arbitrariness, connected primarily with the fact that the width of the transition region between the lit and shadow zones is finite, but the ideal absorber was postulated in accordance with phenomenological considerations of geometrical acoustics where all transition regions are, indeed, of zero width. One could choose z_L such that at $z = 0$ Eq. 91 has decayed to a specified level below Ai(0), thereby placing the plane $z = 0$ "deep" in the shadow zone for $\ell \ll L$. For example, for a decay to about 5 percent of Ai(0), the width of the transition region is

$$z_L \approx 3\left(k_1^2 a\right)^{-1/3} . \tag{94}$$

As the wavelength tends to zero, $k_1 \to \infty$, and z_L approaches zero, in consonance with geometrical acoustics. Alternatively, one can take the transition point z_L coincident with $z = 0$. In this case, the wave function actually penetrates a distance $3\left(k_1^2 a\right)^{-1/3}$ into a region $z < 0$, which, in view of the fact that $z = 0$ should coincide with the planar absorber, appears to carry with it a greater degree of artificiality than that resulting from the placement of the caustic surface above $z = 0$. However, such a picture maintains a closer correspondence with the ray interpretation shown in the illustration on page 40, in that all rays with turning points $z \geq 0$ are included. For this reason the latter point of view will be adhered to herein. Thus, the number of contributing modes L is given implicitly by

$$\sigma_L \approx \left(k_1^2 a\right)^{1/3} h . \tag{95}$$

The residue series now follows from Eqs. 76 and 87, by an argument analogous to that employed in obtaining Eq. 78. Hence, there results

$$\Psi(\rho,z,z') \sim \frac{-m\, e^{-i\pi/4}\, a^{2/3}\, k_1^{-1/6}}{\sqrt{8\pi\rho}} \qquad (96)$$

$$k_1\rho \sim \infty$$

$$\sum_{\ell=L}^{1} \frac{Ai\left[\left(k_1^2 a\right)^{1/3}(h-z) - \sigma_\ell\right]}{Ai(-\sigma_\ell)\,\cos w_\ell \sqrt{\sin w_\ell}}\, e^{ik_1(z'-h)\cos w_\ell + ik_1\rho \sin w_\ell} ,$$

where $\sin w_\ell$ is given by Eq. 91 and

$$\cos w_\ell = \left[1 - N^2 + \sigma_\ell \left(\frac{a}{k_1}\right)^{2/3}\right]^{1/2} . \qquad (97)$$

As is evident from the steps leading to the construction of Eq. 96, the number of terms in the series can be substantially smaller than for a layer of equal height bounded by a perfectly reflecting surface. An estimate of L is readily obtained if the layer height is assumed to be large. Specifically, if

$$\sigma_L = \left(k_1^2 a\right)^{1/3} h \gg 1 , \qquad (98)$$

the zero location σ_L can be related to L with the aid of the asymptotic from Eq. 73a. This yields

$$L\pi \approx \frac{2}{3}\,\sigma_L^{3/2} + \frac{\pi}{4} \approx \frac{2}{3}\,\sigma_L^{3/2} = \frac{2}{3}\, h^{3/2}\, k_1 a^{1/2} ,$$

or

$$L \approx \frac{2}{3\pi}\, k_1\, a^{1/2}\, h^{3/2} . \qquad (99)$$

On the other hand, for a perfectly reflecting layer, the number of terms L_{refl} required in the residue series was shown to be approximately $L_{refl} \approx k_1 hN/\pi$. Thus, the ratio of the number of residue terms for a perfectly absorbent lower boundary to number of terms required to

represent the solution when the layer is bounded by a perfectly reflecting surface is

$$\frac{L}{L_{refl}} \approx \frac{2\sqrt{ah}}{3N} . \qquad (100)$$

To illustrate the magnitude of this ratio by means of a concrete example, consider $a = 1.25 \times 10^{-6}$ (which corresponds to an average isothermal velocity gradient in a deep ocean), $N = 0.228$, and $h = 3000$ meters. One finds that Eq. 100 yields $L/L_{refl} \approx 0.11$, that is, 11 percent of the modes are unaffected by the perfectly reflecting boundary and correspond to a ray system with turning points with $z \geq 0$. These are the only permissible modes in the layer once the perfectly reflecting surface is replaced by the perfect absorber.

For an evaluation of Ψ by means of Eq. 96 near the lower layer boundary, the number of significantly contributing terms in the series will be considerably smaller than L. This is because most of the Airy functions in the numerator will be evaluated below their transition points and, consequently, will be strongly attenuated. As the observation point is moved away from the bottom boundary, transition points of modes with progressively lower indexes will be intercepted, thus necessitating the inclusion of an increasingly larger number of terms in the summation. Only close to the upper layer boundary will the required number of terms approach L. It should, however, be borne in mind that Eq. 96 does not hold at observation points close to the upper medium interface: first, because the excluded saddle point contribution may become significant and, second, because the zeroth-order solution for the roots in Eq. 88 is inadequate for points sufficiently close to $z = h$. Indeed, by virtue of Eq. 88, the numerators in Eq. 96 vanish at $z = h$, yielding $\Psi(h,z',\rho) \equiv 0$, which is evidently incorrect.

To obtain an estimate of the number of significant mode functions in Eq. 96 for observation points close to $z = 0$, one has to solve for the modal index ℓ_{max} of the highest order contributing mode at $z = 0$.

Denoting the width of the transition region by z_L, the zero corresponding to the mode with the transition point at $z = z_L$ is

$$\sigma_{\ell max} = \left(k_1^2 a\right)^{1/3} (h - z_L) \ .$$

It will be assumed that z_L/h is small. Consequently, $\sigma_{\ell max} \gg 1$ whenever $\sigma_L \gg 1$, and one can solve for ℓ_{max} with the aid of the asymptotic form (Eq. 73a). This yields

$$\ell_{max} \approx \frac{2}{3\pi} \left[\sigma_{\ell max}\right]^{3/2} = \frac{2}{3\pi} k_1 a^{1/2} h^{3/2} \left[1 - \frac{z_L}{h}\right]^{3/2} \qquad (101)$$

$$\approx \frac{2}{3\pi} k_1 a^{1/2} h^{3/2} \left(1 - \frac{2}{3} \frac{z_L}{h}\right) ,$$

where the last result follows from the use of the binomial expansion and retention of only the linear term z_L/h. Combining Eq. 101 with Eq. 99, one can write for the ratio of the number of contributing terms to the total,

$$\frac{L - \ell_{max}}{L} \approx \frac{2}{3} \left(\frac{z_L}{h}\right) \ . \qquad (102)$$

Returning to the preceding numerical example, one obtains from Eq. 94 $z_L \approx 246$, which yields $(L - \ell_{max})/L \approx 0.123$, an approximately tenfold reduction from the number of terms required for observation points near the upper boundary.

E. ACOUSTIC POINT SOURCE WITHIN THE PLANAR LAYER

In the following discussion, some of the preceding results will be compared with those for the acoustic potential due to a point source within the planar layer. With reference to the sketch on page 5, let the source be located at z', $0 \le z' \le h$ and $\rho = 0$. The integral representation, Eq. 4, for the acoustic potential still applies, except that the one-dimensional Green's function must be replaced by

$$g(z,z';\varkappa_1) =$$

$$\frac{\{f_2(z_<)\dot{f}_1(o) - \dot{f}_2(o)f_1(z_<)\}}{[f_2(o)\dot{f}_1(o) - \dot{f}_2(o)f_1(o)]} \tag{103}$$

$$\times \frac{\{i\varkappa_1[f_1(z_>)f_2(h) - f_2(z_>)f_1(h)] + m[f_2(z_>)\dot{f}_1(h) - f_1(z_>)\dot{f}_2(h)]\}}{\{i\varkappa_1[\dot{f}_2(o)f_1(h) - \dot{f}_1(o)f_2(h)] + m[\dot{f}_1(o)\dot{f}_2(h) - \dot{f}_2(o)\dot{f}_1(h)]},$$

where $f_{1,2}(z)$ are, as before, any two linearly independent solutions of Eq. 8. The symbols $z_<$ and $z_>$ have the following meanings: if $z < z'$, then $z_< = z$ and $z_> = z'$; if $z' < z$, then $z_< = z'$ and $z_> = z$. Before discussing the various special cases of constant and variable reflective index profiles, it is of interest to consider Eq. 103 for a point source on the boundary $z = h$ within the layer, for arbitrary functional forms $f_{1,2}(z)$. Setting $z_< = z$ and $z_> = z' = h$, and noting that the Wronskian $f_2(z)\dot{f}_1(z) - \dot{f}_2(z)f_1(z)$ is independent of z, yields

$$g(z,h;\varkappa_1) = m \frac{f_2(z)\dot{f}_1(o) - \dot{f}_2(o)f_1(z)}{i\varkappa_1[\dot{f}_2(o)f_1(h) - \dot{f}_1(o)f_2(h)] + m[\dot{f}_1(o)\dot{f}_2(h) - \dot{f}_2(o)\dot{f}_1(h)]}. \tag{104}$$

Comparing Eq. 104 with the Green's function for a point source above the layer, Eq. 7, one notes that the latter differs from Eq. 104 only by the factor $\exp[i\varkappa_1(z' - h)]$. The quantity $\varkappa_1(z' - h) = k_1(z' - h)\cos w$ represents the phase shift along the z direction between the source location and the upper medium interface for a plane wave incident at an angle w relative to the z axis. Representations for the acoustic potential such as Eqs. 4 or 46 can be interpreted as superposition integrals of plane waves launched by the point source into the layer at all possible directions of incidence. Not all directions of incidence are equally effective in contributing significantly to the acoustic potential at a given observation point within the layer. For

example, when the observation point is at a large radial distance from the source point, only plane waves whose angles of incidence fall within a narrow range may contribute significantly. In such cases, cosw may be treated as a constant, and exp $i[k_1(z' - h)\cos w]$ factored out of the superposition integral. Under these circumstances, substitution of Eqs. 7 or 104 into Eq. 4 leads to the same magnitude of acoustic potential. Thus, one obtains the following source equivalent principle: if cosw $\approx$ constant for all significantly contributing wave types, a point source of unit strength above the layer produces the same magnitude of acoustic potential within the layer as that produced by a point source of unit strength at the upper interface within the layer. Evidently, if the preceding condition holds, the magnitude of the acoustic potential in the layer is not dependent on the source height above the medium interface. A particular case in which this source equivalence principle applies is a layer of constant refractive index with $2n^2 << 1$ and $m << 1$, as discussed in conjunction with Eq. 68. This is readily generalized to a layer with a linearly decreasing refractive index profile and a perfectly reflecting lower boundary by replacing n with N, the relative refractive index at the upper medium interface. When the lower layer boundary is replaced by a perfect absorber, the condition for source equivalence follows by requiring that $\cos w_\ell$ in Eq. 97 be independent of ℓ. This will be the case if

$$1 - N^2 >> \sigma_L \left(\frac{a}{k_1}\right)^{2/3} . \tag{105}$$

For large h, one can employ Eq. 98 to obtain

$$1 - N^2 >> ha. \tag{106}$$

Note that for a perfectly absorbent boundary, unlike for a perfectly reflecting boundary, the constraint $2N^2 << 1$ is superfluous.

To obtain a residue series for the acoustic potential produced by a point source within the layer, one starts with the integral representation analogous to Eq. 46, namely,

$$\Psi(\rho,z,z') = \frac{k_1^2}{4\pi}\sqrt{\frac{2}{\pi k_1\rho}}\, e^{-i\pi/4}\int_P \sqrt{\sin w}\,\cos w\;\; g(z,z';w)\, e^{ik_1\rho\cos w}\, dw\ , \qquad (107)$$

where $g(z,z';w)$ is given by Eq. 103 with the transformation $\kappa_1 = k_1\cos w$. For a constant refractive index profile, Eq. 103 reduces to

$$g(z,z';w) = \frac{\cos(\kappa_2 z_<)\,\{-\kappa_1\sin[\kappa_2(z_>-h)] + i m\,\kappa_2\cos[\kappa_2(z_>-h)]\}}{\kappa_2[\kappa_1\cos\kappa_2 h - i m\,\kappa_2\sin\kappa_2 h]}\ ,$$

$$\kappa_1 = k_1\cos w,\ \kappa_2 = k_1\sqrt{n^2-\sin^2 w}\ . \qquad (108)$$

The asymptotic evaluation of Eq. 107 for large ρ proceeds exactly as in Eq. 46, with the steepest descents path following the curve shown in the illustration on page 25 with $\theta = \pi/2$. At observation points not too close to $z = h$, the contribution from the saddle point at $\theta = \pi/2$ is again found to be exponentially small by comparison with the residue series, which in the present case may be written

$$\Psi(\rho,z,z') \sim \frac{2\pi i k_1^2}{4\pi}\sqrt{\frac{2}{\pi k_1\rho}}\; e^{-i\pi/4} \qquad (109)$$

$$k_1\rho \sim \infty$$

$$\sum_\ell \frac{\sqrt{\sin w_\ell}\,\cos w_\ell}{\kappa_{2\ell}}\; e^{ik_1\rho\sin w_\ell}$$

$$\times \frac{\cos(\kappa_{2\ell} z_\ell)\{-\kappa_{1\ell}\sin[\kappa_{2\ell}(z_>-h)] + i m\,\kappa_{2\ell}\cos[\kappa_{2\ell}(z_>-h)]\}}{\frac{d}{dw}\{k_1\cos w\cos\kappa_2 h - i m\,\kappa_2\sin\kappa_2 h\}_{w=w_\ell}}\ .$$

Employing the zeroth order approximation for the roots when $m \ll 1$, Eq. 109 simplifies to

$$\Psi(\rho,z,z') \sim \frac{2\pi i}{4\pi h}\sqrt{\frac{2}{\pi k_1 \rho}}\, e^{-\pi/4}\left\{\sum_{\ell=0}^{\infty} \frac{\cos(\kappa_{2\ell} z)\cos(\kappa_{2\ell} z')}{\sqrt{\sin w_\ell}}\, e^{ik_1 \rho \sin w_\ell}\right.$$

$$\left. + im\sum_{\ell=0}^{\infty} \frac{\kappa_{2\ell}\cos(\kappa_{2\ell} z_<)\sin(\kappa_{2\ell} z_>)}{k_1 \cos w_\ell \sqrt{\sin w_\ell}}\, e^{ik_1 \rho \sin w_\ell}\right\}, \qquad (110)$$

where

$$\kappa_{2\ell} = \frac{(2\ell + 1)\pi}{2h} .$$

The first sum in Eq. 110 is the modal expansion for an impenetrable upper boundary, that is, $m = 0$, equivalent to the boundary condition $\Psi(\rho,h,z') = 0$. Hence, this sum vanishes when the source is placed at the upper layer boundary, in which case the second sum constitutes the dominant contribution. Indeed, for $z' = z_> = h$, the second sum reduces to Eq. 65, except for the factor $\exp[ik_1(z' - h)\cos w_\ell]$ multiplying each mode function. If $\cos w_\ell \approx$ constant for all pertinent modal indexes, the exponential factor may be brought outside the summation, thus yielding the source equivalence discussed in the preceding. As the source location is moved away from the medium interface, the first sum in Eq. 65 begins to dominate. A residue series analogous to Eqs. 109 or 110 can be obtained for the linearly decreasing refractive index profile by employing the Airy functions Eqs. 13a and 13b in 103. When the lower boundary is perfectly absorbent and $m \ll 1$, the approximate form of the residue series is

$$\Psi(\rho,z,z') \sim -e^{-i\pi/4}\sqrt{\frac{\pi k_1}{8\rho}}\, a^{1/3}\, k_1^{-4/3} \tag{111}$$

$$\left\{\sum_{\ell=L}^{1} \frac{ik_1 Bi(-\sigma_\ell)}{\dot{A}i(-\sigma_\ell)} \frac{e^{ik_1\rho\sin w_\ell}}{\sqrt{\sin w_\ell}} Ai\left[\left(k_1^2 a\right)^{1/3}(h-z)-\sigma_\ell\right] Ai\left[\left(k_1^2 a\right)^{1/3}(h-z')-\sigma_\ell\right]\right.$$

$$-m\left(k_1^2 a\right)^{1/3}\sum_{\ell=L}^{1} \frac{e^{ik_1\rho\sin w_\ell} Ai\left[\left(k_1^2 a\right)^{1/3}(h-z_<)-\sigma_\ell\right]}{\cos w_\ell \sqrt{\sin w_\ell}\, \dot{A}i(-\sigma_\ell)} \left(\dot{A}i(-\sigma_\ell) Bi\left[\left(k_1^2 a\right)^{1/3}(h-z_>)-\sigma_\ell\right]\right.$$

$$\left.\left. -\dot{B}i(-\sigma_\ell) Ai\left[\left(k_1^2 a\right)^{1/3}(h-z_>)-\sigma_\ell\right]\right)\right\}$$

The two sums in Eq. 111 admit the same interpretation as in Eq. 110: the first sum is the guided mode series for an impenetrable upper boundary. This sum represents the dominant contribution if the source point z' is not too close to h, and vanishes identically for $z' = h$. In this case, the second sum dominates. Upon setting $z_> = z' = h$ and employing the identity $\dot{A}i(-\sigma_\ell)\, Bi(-\sigma_\ell) - Ai(-\sigma_\ell)\, \dot{B}i(-\sigma_\ell) = -1/\pi$, one obtains Eq. 96 (apart from the exponential factor $\exp ik_1(z'-h)\cos w_\ell$), in consonance with the source-equivalence principle.

The computational aspects associated with Eq. 111 are identical to those considered in Section D of Chapter II in conjunction with the point source within the layer.

III. PROPAGATION OF ACOUSTIC SIGNALS OVER LONG PATHS BELOW THE OCEAN SURFACE

The previously derived residue-series representations will be applied to estimating the acoustic pressure produced in an isothermal ocean, at large distances from a single frequency source above the ocean surface. Even though the two simplified planar models discussed, viz., the one bounded by a perfectly rigid reflecting flat surface and the other bounded by a perfectly absorbent surface, pertain to grossly idealized situations having no counterpart in the case of a real ocean floor, they correspond to limiting cases and, as such, can be of value in providing bounds on possible acoustic signal enhancement arising from systematic ocean floor reflections. Also, such models can yield quantitative estimates of relative signal strength produced by sources above and below the ocean interface. In all cases, the observation point (receiver) will be located deep below the ocean surface in the isothermal layer, well below the seasonal and main thermoclines. The linearly increasing velocity profile of the isothermal sea will be assumed to extend up to the ocean surface. The variation of the acoustic velocity with depth is expressed by

$$c_2(z) = c_2(h)\,[1 + \alpha(h-z)]\ , \tag{112}$$

where $c_2(h)$ is the speed of sound at the ocean surface. Since the slope parameter $\alpha(\alpha > 0)$ is small, the linear increase of velocity with depth corresponds, within a good approximation, to a linearly decreasing refractive index profile. Thus, the previously employed slope parameter (a) is related to α by

$$\alpha = \frac{a}{2N^2}\ , \tag{117}$$

(compare Eq. 10) where N is the ratio of the speed of sound in air to that in the water immediately below the interface, that is,

$$N = \frac{c_1}{c_2(h)} = \frac{k_2(h)}{k_1} \quad .$$

In the following discussion the sound speed in air will be taken as 340 m/sec, while $c_2(h) = 1490$ m/sec, yielding $N \cong 0.228$. A suitable average value of the slope parameter is $a = 1.25 \times 10^{-6}$/m (Ref. 2). The source frequency of interest is below 100 Hz. In particular, for all subsequent numerical results a frequency of 65 Hz will be assumed, yielding the wavenumber $k_1 = \frac{2\pi}{\lambda_1} = \frac{w}{c_1} = 1.2$.

The analysis in Chapter II dealt exclusively with the potential function Ψ, produced by a unit point source. In discussing acoustic signal strength, it is customary to employ the acoustic pressure which is proportional to the product of the medium density and the potential function (Eq. 2). Comparison of acoustic pressure produced by sources within and outside the water will be facilitated by introducing the following notation. Let p_{21} denote the pressure at an observation point in medium 2 (water) due to a point source in medium 1 (air). The strength of the source is such that at an observation point 1 meter from the (isolated) source in air the pressure is P_1. Similarly, let p_{22} be the pressure in medium 2 due to a point source in medium 2, with an isolated source strength yielding a pressure P_2 at a 1-meter distance. With Ψ_{21} and Ψ_{22} the potential in medium 2 produced by unit point sources located in mediums 1 and 2, respectively, one can write by virtue of Eq. 2,

$$p_{21} = \frac{4\pi}{m} P_1 \Psi_{21} \, , \qquad (114a)$$

$$p_{22} = 4\pi P_2 \Psi_{22} \, , \qquad (114b)$$

where $m \cong 1/800$ is the water to air density ratio. In applying Eq. 114 to the same observation point in the water, it is instructive to consider the ratio

$$\frac{P_{21}}{P_{22}} = \frac{P_1}{mP_2} \cdot \left(\frac{\Psi_{21}}{\Psi_{22}}\right) . \qquad (115)$$

One notes that if $\Psi_{21} = \Psi_{22}$, the pressure produced in the water by a source in air is 800 times that which arises from a source of equal strength located in the water. As was shown in Chapter II, Section E, a unit strength source within the layer at the medium interface gives rise to a potential at large radial distances from the source approximately equal that due to a unit source above the layer. This equivalence principle holds if $m << 1$ and $N^2 << 1$, conditions well satisfied by the physical constants given above. Thus, a point source above the ocean surface appears to couple acoustic pressure to distant observation points more efficiently than a source in the ocean close to the surface*. This result obtains only for locations of the submerged source close to the interface (a fraction of a wavelength), and is due to the almost perfect reflecting properties of the assumed smooth air-water interface, giving rise to a partial cancellation of the source with its image. As the source is moved away from the interface, the acoustic potential increases. However, by virtue of Eq. 115, Ψ_{22} must increase by a factor $\frac{1}{m}$ (that is, 800) for the pressure at a distant observation point of two equal strength sources (one above, the other below the interface) to be just equal.

Results of calculation of the acoustic potential for a perfectly reflecting rigid lower boundary are shown in Figs. 2 through 5. The computations were performed by summing the leaky wave series for a constant refractive index profile [$n(z) = N \approx 0.228$] as given by Eq. 63. The iteration scheme for the determination of the leaky wave poles

*This relation does not apply to acoustic power densities (intensities) in the two media.

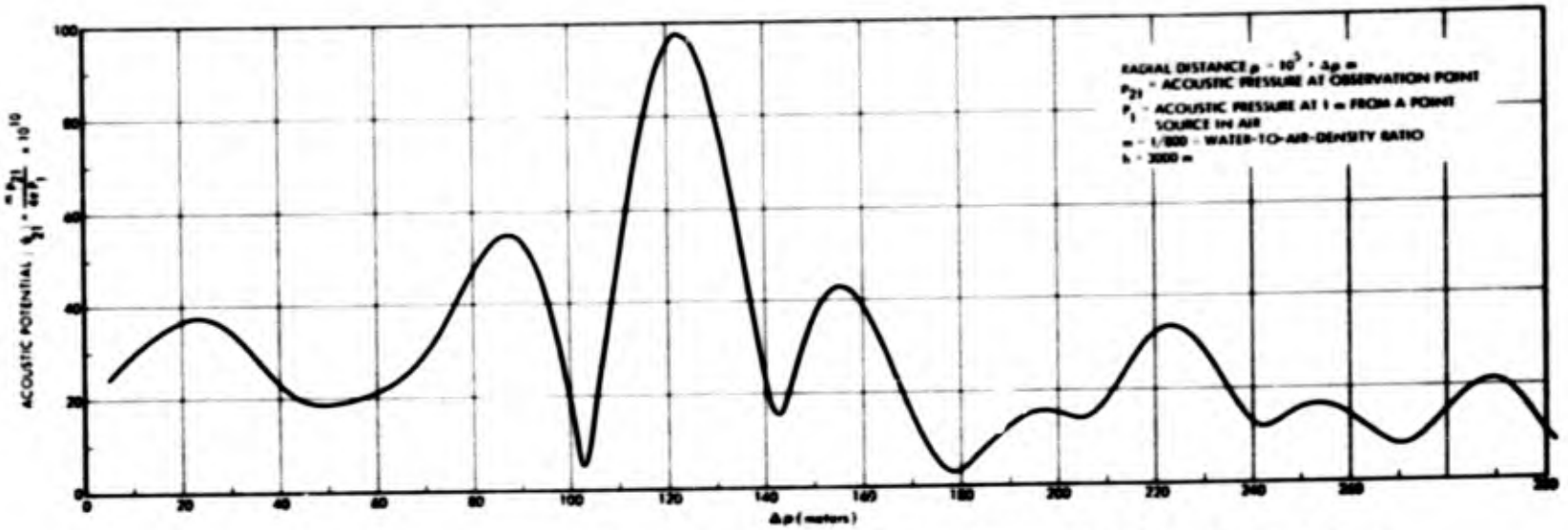

FIGURE 2. Acoustic Potential as a Function of Radial Distance Along the Ground Plane from a Point Source 3000 m Above the Air/Water Interface

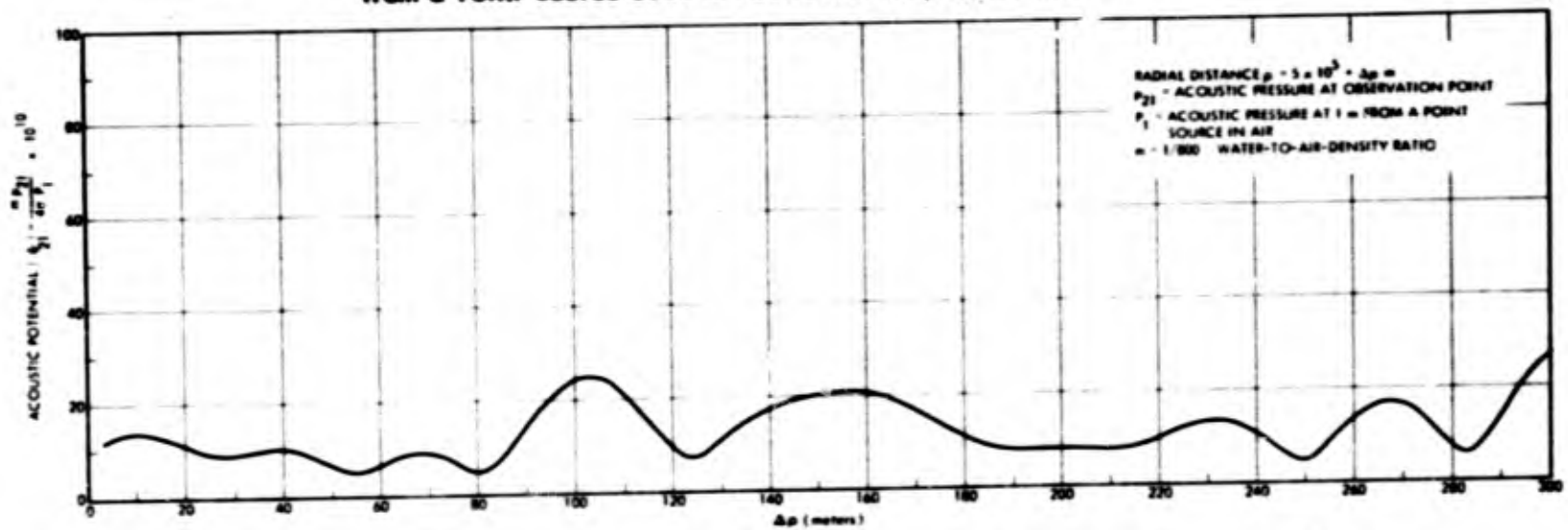

FIGURE 3. Acoustic Potential as a Function of Radial Distance Along the Ground Plane for a Point Source at 3000 m Above the Air/Water Interface

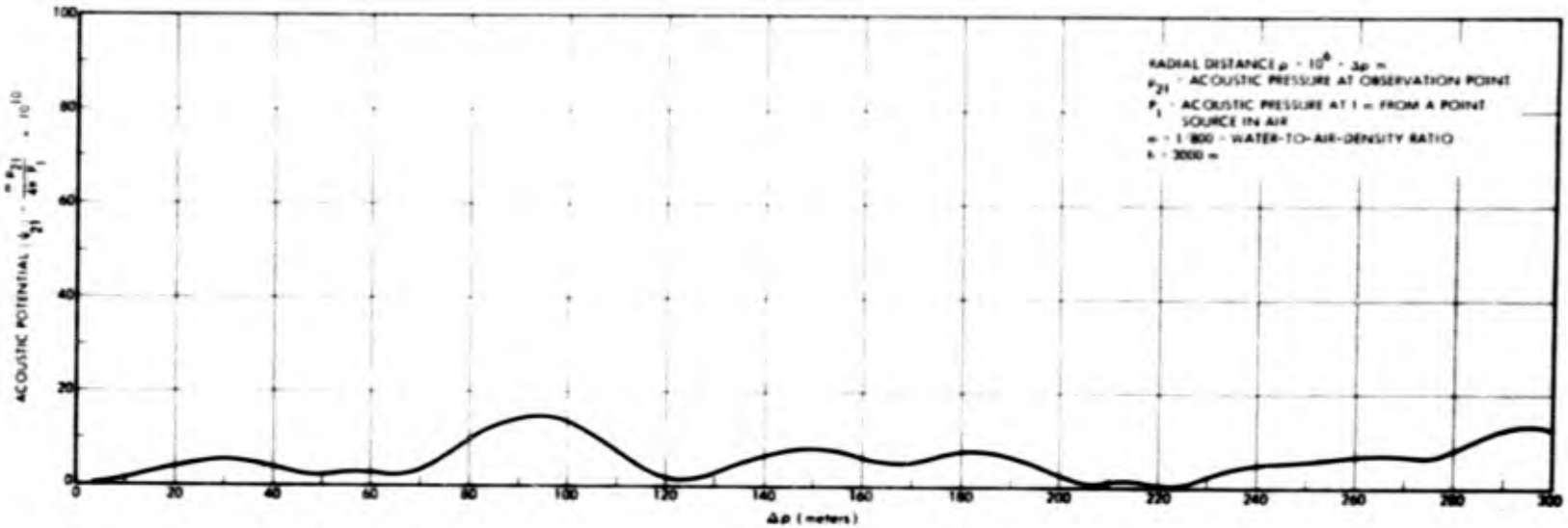

FIGURE 4. Acoustic Potential as a Function of Radial Distance Along the Ground Plane from a Point Source 3000 m Above the Air/Water Interface

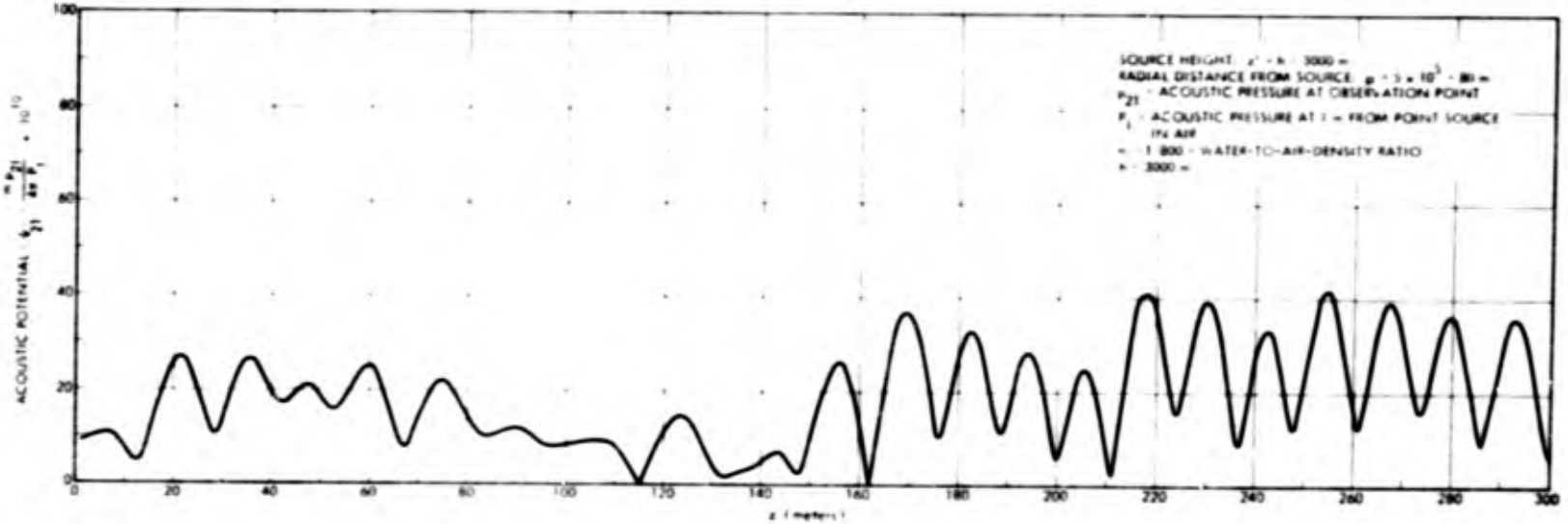

FIGURE 5. Acoustic Potential as a Function of Location of Observation Points Above Ground Plane

outlined in Eqs. 55 and 56 was found to converge extremely rapidly, and to the precision attainable within the scale range of the plots in Figs. 2 through 5, the results are not distinguishable from those obtained by means of the somewhat simpler series, Eq. 65, based on the zeroth-order approximation to the roots. The number of terms required in the series was only slightly larger than the estimate $L_{refl} \approx Nk_1h/\pi \approx 260$, which follows by requiring the radicand in Eq. 56a to vanish. Figs. 2 through 4 show plots of acoustic potential along the ground plane ("ocean floor") vs. the radial distance from the source (compare the illustration on page 5) located 3000 meters above the air-water interface. Due to the fine-grained fluctuations with ρ (periods of approximately 10 meters), the potential was plotted only at three selected range "windows" of 300 meters, starting at 100, 500, and 1000 km. The complicated interference patterns are due to multiple-phase cancellations and reinforcements of about 260 modes. Modes with highest indexes contribute to oscillations with highest spatial frequencies, and correspond to rays with nearly normal incidence undergoing multiple reflections between the lower and upper boundary. Even though each individual mode amplitude decays as $1/\sqrt{\rho}$, the decay of the composite wave function does not appear characterisable by a simple decay law. Figure 6 shows the variation of the potential function, with height measured from the bottom boundary at a range of 500 km + 80 m, deliberately chosen to correspond to one of the minima in Fig. 3. At this range, the variation of acoustic potential with distance above the bottom boundary for a source in the water ($z' = 1500$) is shown in Fig. 6. Comparing the value of $|\Psi|$ with that in Fig. 5, one notes that on the "average" the potential due to the submerged source of unit strength is greater by about a factor of 1000 than that due to a unit source above the interface. This result differs substantially from that which obtains for a submerged source near the interface, where the acoustic potentials of the above-surface and submerged equal-strength sources were shown to be nearly equal. Thus, in view of Eq. 115, the "average" pressure due to a submerged source is of the same order of magnitude as that arising from an above-surface

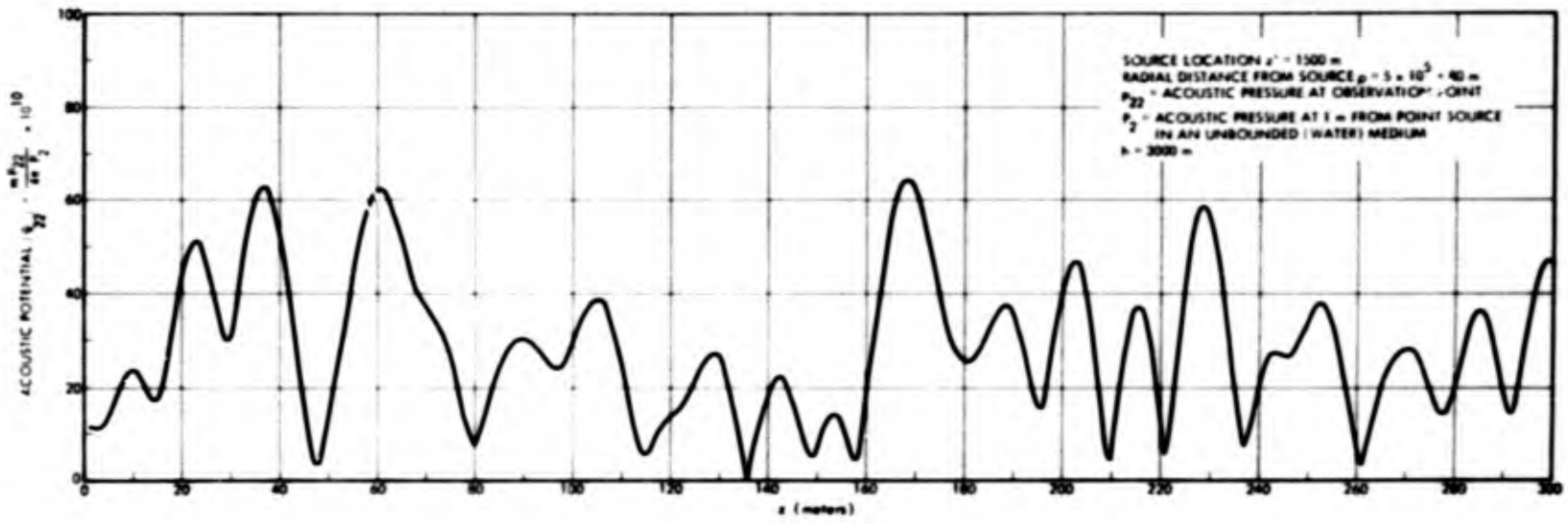

FIGURE 6. Acoustic Potential as a Function of Location Observation Points Above Ground Plane for a Point Source in the Water

source of equal strength. Although this "average" source equivalence is inferred from an examination of results of a detailed calculation for a layer with a constant refractive index profile, it is expected to hold for a layer with a linearly decreasing refractive index profile when the slope parameter (a) is small. For $a = 1.25 \times 10^{-6}$/m, only a relatively small fraction of the total number of rays will fail to be reflected by the lower boundary (about 11 percent according to Eq. 110). Rays reflected from the lower boundary will give rise to a phase interference pattern differing from that in Figs. 2 through 6 only in respect to detail in the fine structure of the spatial oscillations but not in the "average" behavior.

The computational aspects of the summation of a residue series, whether for a constant or variable refractive index profile, are quite similar, and results of such calculations provide in detail the fine structure fluctuations of the acoustic pressure at large distances from the source. However, due to inevitable spatial and temporal inhomogeneities of the constitutive parameters of the ocean, the complicated interference patterns of Figs. 2 through 6 would generally not be experimentally observable, but only their averages. Thus, it is desirable to establish an average measure of acoustic pressure. In particular, such an average measure should facilitate the description of decay (spreading) of the acoustic pressure with ρ. As is evident from Figs. 2 through 4, a simple decay law with range cannot be directly inferred from the data. The acoustic pressure in a layer with a constant refractive index and a reflecting lower boundary, averaged over all modes with respect to all observation points z and source locations z' within the layer, decays at $1/\rho^{3/4}$, a decay law falling in between pure cylindrical ($1/\sqrt{\rho}$) and pure spherical ($1/\rho$) spreading (Ref. 2, p. 415). The averaging procedure employed in Ref. 2 does not appear to apply to a source above the layer nor to a variable refractive index profile with a strongly reflecting lower boundary. However, if the lower layer boundary is assumed perfectly absorbent, the average pressure will be shown to obey the cylindrical spreading law ($1/\sqrt{\rho}$) for a source within or outside the layer. Moreover,

expressed in terms of these average quantities, an equivalence principle for sources within and outside the layer can be phrased in a particularly simple form.

Assuming a perfectly absorbent "ocean floor" and a depth h, an average acoustic potential due to a unit source above the ocean surface may be defined by

$$\overline{\Psi_{21}(\rho)} = \left[\frac{1}{h}\int_{-\infty}^{h} |\Psi_{21}(\rho,z,z')|^2 \, dz\right]^{\frac{1}{2}} , \qquad (116)$$

where $\Psi_{21}(\rho,z,z')$ is given by the residue series (Eq. 96). The average in Eq. 116 is taken over all observation points at a fixed radial distance from the source. Strictly speaking, the integration should extend only over the finite interval $0 \le z \le h$. However, since the Airy functions in Eq. 97 decay exponentially for $z < 0$, the integration can be extended to $-\infty < z < h$ with only a negligible error. This extension will permit use of an orthogonality relation for Airy functions, thereby leading to a considerable simplification in the final results. In parallel with Eq. 116, one can also define an average acoustic potential due to a unit source in the ocean. Thus,

$$\overline{\Psi_{22}(\rho)} = \left[\frac{1}{h^2}\int_{-\infty}^{h}\int_{-\infty}^{h} |\Psi_{22}(\rho,z,z')|^2 \, dz, \, dz'\right]^{\frac{1}{2}} , \qquad (117)$$

where $\Psi_{22}(\rho,z,z')$ is given by the first series* in Eq. 111 and the average is taken over all observation points z <u>and</u> source points z' within the layer. The extension of the integration interval to $-\infty < z' < h$ can again be justified on the basis of exponential decay of the Airy functions for $z' < 0$. It may be shown that the Airy functions $\mathrm{Ai}\left[(k_1^2 a)^{1/3}(h-z) - \sigma_\ell\right]$, $\ell = 1, 2 \ldots$ form a complete

*The second series of Eq. 111 contributes significantly only at source points very close to the interface and can be neglected in Eq. 117.

orthonormal set over the interval* $-\infty < z \le h$. The orthogonality may be expressed as

$$\int_{-\infty}^{h} \mathrm{Ai}\left[\left(k_1^2 a\right)^{1/3}(h-z) - \sigma_\ell\right] \mathrm{Ai}\left[\left(k_1^2 a\right)^{1/3}(h-z) - \sigma_k\right] dz \qquad (118)$$

$$= \frac{\dot{\mathrm{Ai}}(-\sigma_\ell)}{\pi\left(k_1^2 a\right)^{1/3} \mathrm{Bi}(-\sigma_\ell)} \delta_{\ell k} ,$$

whose $\delta_{\ell k}$ is the Kronecker symbol. With the aid of Eq. 118, the averages of Eqs. 116 and 117 are readily evaluated. Inserting Eq. 96 into Eq. 116 and noting that for the small slope parameter of interest $\sin w_\ell$ and $\cos w_\ell$ (appearing in Eq. 96 as mode-amplitude factors) may be replaced by N and $(1 - N^2)^{\frac{1}{2}}$, respectively, yields

$$\overline{\Psi_{21}(\rho)} = m\sqrt{\frac{aL}{8\pi k_1 hN(1-N^2)}} \left(\frac{1}{\sqrt{\rho}}\right) , \qquad (119)$$

where L is the number of modes entering in the summation, Eq. 96. When L is approximated by Eq. 99, Eq. 119 may be written

$$\overline{\Psi_{21}(\rho)} \cong \frac{m}{\pi\sqrt{12N(1-N^2)}} (a^3 h)^{\frac{1}{4}} \left(\frac{1}{\sqrt{\rho}}\right) . \qquad (120)$$

Similarly, substituting the appropriate series for $\Psi_{22}(z,z',\rho)$ in Eq. 117 results in

$$\overline{\Psi_{22}(\rho)} = \frac{1}{h}\sqrt{\frac{L}{8\pi k_1 N}} \left(\frac{1}{\sqrt{\rho}}\right), \qquad (121)$$

---

*This may readily be proven by first finding the Green's function satisfying

$$\left[\frac{d^2}{dz^2} + \lambda - ak_1^2(h-z)\right] g(z,z';\lambda) = -\delta(z-z'), \quad -\infty < z,z' < h$$

with $g(h,z';\lambda) = 0$ and $g(z,z';\lambda) \to 0$ $|z-z'| \to \infty$, and recovering the completeness relationship from an integration of $g(z,z';\lambda)$ in the complex λ plane.

and again using Eq. 99, one obtains

$$\overline{\Psi_{22}(\rho)} \cong \frac{1}{\pi\sqrt{12N}} \left(\frac{a}{h}\right)^{\frac{1}{4}} \left(\frac{1}{\sqrt{\rho}}\right) . \tag{122}$$

Equations 120 and 122 constitute the desired formulas for average acoustic potentials. Note that these are independent of k_1, and hence of the frequency of the source. To compare the relative average magnitudes of acoustic pressure produced by a source within the layer with that produced by a source above the layer, one can employ Eq. 115 together with Eqs. 121 and 122 to obtain

$$\frac{\bar{P}_{21}}{\bar{P}_{22}} = \left(\frac{P_1}{P_2}\right)\sqrt{\frac{ah}{1-N^2}} . \tag{123}$$

For a layer height of 3 km [(as in Figs. 2 through 6) $a = 1.25 \times 10^{-6}/m$ and $N = 0.228$] Eq. 123 shows that for equal source strengths the average pressure due to the source above the ocean surface is only about 6 percent of that produced by the source below the ocean surface. This is to be contrasted with the result for a perfectly reflecting ocean bottom, where the pressures due to the two sources were found to be about equal. Evidently, the reflecting properties of the bottom contribute to a substantial reinforcement of the acoustic signal when the source is located above the layer.

REFERENCES

1. R. J. Urick, Principles of Underwater Sound for Engineers, McGraw-Hill, 1967.

2. L. M. Brekhovskikh, Waves in Layered Media, Academic Press, New York, 1960.

3. L. B. Felsen and N. Marcuvitz, Radiation and Scattering of Waves, Prentice Hall, 1973.

4. M. Abramowitz and I. Stegun, Handbook of Mathematical Functions, NBS Applied Math. Series 55, 1964.